nature cancer

Article

https://doi.org/10.1038/s43018-024-00870-6

TIGIT and PD-L1 co-blockade promotes clonal expansion of multipotent, non-exhausted antitumor T cells by facilitating co-stimulation

Received: 1 April 2024

Accepted: 28 October 2024

Published online: 16 December 2024

Check for updates

Katherine Nutsch[1,2], Karl L. Banta[1,2], Thomas D. Wu[1,2], Charles W. Tran[1], Stephanie Mittman[1], Ellen Duong[1], Barzin Y. Nabet[1], Yan Qu[1], Katherine Williams[1], Sören Müller[1], Namrata S. Patil[1], Eugene Y. Chiang[1,3] ✉ & Ira Mellman[1,3] ✉

Blockade of immune checkpoints PD-1 and TIGIT has demonstrated activity in mouse tumor models and human patients with cancer. Although these coinhibitory receptors can restrict signaling in CD8$^+$ T cells by regulating their associated co-stimulatory receptors CD28 and CD226, the functional consequences of combining PD-1 and TIGIT blockade remain poorly characterized. In mouse tumor models, we show that combination blockade elicited CD226-driven clonal expansion of tumor antigen-specific CD8$^+$ T cells. The expanded clones emerged from a population of stem-like cells in draining lymph nodes, entering the blood as a previously unidentified single-phenotype, multiclonal population. Upon reaching the tumor, these transiting cells expanded further and differentiated into effector or exhausted T cells, with combination blockade restricting entry into the exhaustion pathway by favoring co-stimulation. Thus, PD-1 and TIGIT inhibition helps shape the repertoire of tumor-reactive CD8$^+$ T cells in draining lymph nodes and determines their immunological fate in the tumor to enhance therapeutic benefit. Analysis of clinical trial samples suggests a similar mechanism may also occur in patients with cancer.

Immunotherapies targeting the PD-1–PD-L1 pathway have shown promise, but only ~30% of patients achieve durable responses, necessitating new strategies such as combinations targeting multiple or novel immune checkpoint receptors[1]. TIGIT (T cell immunoreceptor with Ig and immunoreceptor tyrosine-based inhibitory domains) has garnered attention due to efficacy in early clinical trials using blocking antibodies against both TIGIT and PD-L1 (ref. 2). Recent analysis of the randomized phase 2 CITYSCAPE trial (NCT03563716) evaluating atezolizumab versus anti-TIGIT monoclonal antibody tiragolumab plus atezolizumab in non-small cell lung cancer (NSCLC)[3] revealed that high baseline intratumoral macrophages and regulatory T (T_{reg}) cells were associated with clinical benefit[4]. Although these results suggest that TIGIT–PD-L1 co-blockade reprograms the tumor microenvironment (TME), high levels of CD8$^+$ effector T (T_{eff}) cells were also associated with response.

In CD8$^+$ tumor-infiltrating lymphocytes (TILs), TIGIT and PD-1 expression are highly correlated[5]. Whereas PD-1 primarily regulates co-stimulation by CD28, TIGIT and PD-1 together regulate the function of CD226, the activating counterreceptor to TIGIT[6]. Coexpression may define distinct populations of 'stem cell-like memory (T_{scm})'

[1]Genentech, South San Francisco, CA, USA. [2]These authors contributed equally: Katherine Nutsch, Karl L. Banta, Thomas D. Wu. [3]These authors jointly supervised this work: Eugene Y. Chiang, Ira Mellman. ✉e-mail: chiang.eugene@gene.com; ira.mellman@ucsf.edu

cells[7–10] believed to be primary targets of PD-1–PD-L1 blockade in both antitumor and antiviral immunity[11–13]. Blocking PD-1 signaling may differentiate these progenitors into T cells with cytolytic effector activity against tumor cells, perhaps via a transient population of T precursor exhausted cells (T_{pex})[14–18]. Thus, PD-1 expression may reflect T cell activation status in addition to denoting exhaustion or commitment to exhaustion. It remains uncertain whether T_{pex} cells give rise to only exhausted T (T_{ex}) cells in the tumor, whether commitment to the T_{ex} pathway begins in draining lymph nodes (dLNs) or whether T_{ex}, T_{eff} and T effector memory (T_{em}) cells originate from separate precursors either before or following tumor arrival. The extent to which checkpoint blockade, especially the role of TIGIT blockade alone or in combination with PD-1 blockade, reprograms $CD8^+$ T cells already committed to the exhaustion pathway or discourages developmental commitment to exhaustion also remains a key unknown[19].

To inform these questions, we utilized a multicompartment, multi-omics single-cell approach, analyzing over 245,000 T cells. We examined not only the features of $CD8^+$ T cells in dLNs and tumors, as has been carried out previously, but also in the blood. Sampling these three critical tissue compartments facilitated insight into the spatial and temporal effects of TIGIT and PD-1 blockade on T cell fate decisions.

Results

Combination treatment requires trafficking of lymphocytes from dLNs to tumor

The coordinate regulation of T cell co-stimulation by PD-1 and TIGIT suggests that both receptors may activate T cells at the same steps and anatomical sites[9]. Using the CT26 syngeneic mouse tumor model, we evaluated the role of dLNs in TIGIT blockade by restricting trafficking of T cells with FTY720, an inhibitor of T cell egress from lymphoid organs[20]. Consistent with previous observations[5], the combination of anti-TIGIT with anti-PD-L1 demonstrated therapeutic efficacy, whereas anti-PD-L1 or anti-TIGIT monotherapies had only limited impact on tumor growth (Fig. 1a and Extended Data Fig. 1a). FTY720 reduced the activity of both single-agent anti-TIGIT and TIGIT–PD-L1 co-blockade (Fig. 1a). Similar results were observed in the EO771 tumor model (Extended Data Fig. 1b).

Treatment with anti-PD-L1, anti-TIGIT, or both did not affect total numbers of $CD8^+$ T cells, $CD4^+$ T cells or T_{reg} cells in CT26 dLNs or tumor, either with or without FTY720 treatment (Extended Data Fig. 1c). We therefore asked whether checkpoint blockade and FTY720 affected the abundance or distribution of tumor antigen-specific $CD8^+$ T cells, identified using tetramers that bind T cell receptors (TCRs) specific for gp70, a tumor-associated, immunodominant retroviral antigen expressed by CT26 cells[21] (Extended Data Fig. 2a). Anti-TIGIT in combination with anti-PD-L1 increased the fraction of $gp70^+CD8^+$ T cells ($P = 0.0138$) in dLNs, whereas anti-PD-L1 or anti-TIGIT alone had little effect (Fig. 1b). The addition of FTY720 before combination treatment further increased the frequency of $gp70^+CD8^+$ T cells in dLNs ($P = 0.0472$), likely reflecting their accumulation in dLNs by preventing T cell egress.

In blood, numbers of $gp70^+CD8^+$ T cells were significantly increased with anti-TIGIT ($P = 0.0134$) or combination treatment ($P < 0.001$), but not in FTY720-treated animals (Fig. 1b). In tumors, only the combination of anti-TIGIT and anti-PD-L1 significantly increased the fraction of $gp70^+CD8^+$ T cells ($P = 0.0098$) (Fig. 1b). As trafficking via blood was blocked, at least some expansion of intratumoral T cells was likely to have occurred locally. Although FTY720-treated mice exhibited a trend toward increased $gp70^+CD8^+$ T cells in tumors, these presumably locally expanded cells were unable to control tumor growth.

We next asked whether antitumor efficacy relied on the continuous recruitment of newly generated T cells from dLNs and blood. Early administration of FTY720 blocked combination efficacy, whereas delaying the blockade of T cell egress until 7 days after combination treatment resulted in only slight impairment in antitumor efficacy (Fig. 1c). Thus, the efficacy of combination checkpoint blockade depends on the induction of tumor-specific $CD8^+$ T cells in dLNs that then traffic to and infiltrate tumors via the circulation. Once the newly mobilized T cells seeded tumors, they were sufficient to sustain therapeutic benefit in response to TIGIT–PD-L1 co-blockade.

CD226 has a role in tumor-specific $CD8^+$ T cell differentiation

As human TILs in NSCLC differentially express CD226 and CD28 in various $CD8^+$ T cell clusters, combination treatment may be required to optimally activate the entire tumor-reactive TIL repertoire[6]. To evaluate the role of CD226 on tumor-specific $CD8^+$ T cell subsets, we segregated $gp70^+CD8^+$ T cells based on CD226 expression. Anti-TIGIT alone or in combination with anti-PD-L1 increased the frequency of $CD226^+gp70^+CD8^+$ T cells in both dLNs and tumors, even with FTY720 treatment (Fig. 2a). Following combination blockade, $CD226^+gp70^+CD8^+$ T cells were substantially more proliferative ($Ki67^+$), but only in dLNs (Fig. 2b,c and Extended Data Fig. 3a). $CD226^-gp70^+CD8^+$ T cell proliferation was not affected by any treatment. Few $CD226^+gp70^+CD8^+$ T cells in dLNs were naive compared to the $CD226^-$ fraction (Fig. 2b and Extended Data Fig. 3b); only combination treatment increased the frequency of $CD226^+gp70^+CD8^+$ T cells with a T_{eff} or T_{em} phenotype, whereas no effects were observed in the $CD226^-$ population (Fig. 2b and Extended Data Fig. 3c).

To further elucidate the effects of checkpoint blockade on activation and differentiation, we measured various markers of T cell states. Slamf6 and TCF1 coexpression delineate T_{scm} or T_{pex} cells[9,19]. In dLNs, the frequency of these cells in the $CD226^+$ fraction was not affected by any treatment, but anti-TIGIT alone or in combination with anti-PD-L1 significantly reduced frequencies in the $CD226^-$ subset (Fig. 2b and Extended Data Fig. 3d; $P = 0.0014$). By contrast, in tumors, anti-TIGIT and combination treatment increased frequencies of $Slamf6^+TCF1^+$ cells in both $CD226^+$ and $CD226^-$ subsets (Fig. 2c and Extended Data Fig. 3d; $P = 0.0014$).

As T cells differentiate from the T_{scm} or T_{pex} state, they express immune checkpoints such as Tim3. Combination treatment as well as anti-TIGIT alone increased the frequencies of both $CD226^+$ and $CD226^-$ $TCF1^+Tim3^+gp70^+CD8^+$ T cells in tumor, whereas effects in the dLNs were limited to the $CD226^+$ subset; FTY720 largely abolished these effects (Fig. 2b,c; see Extended Data Fig. 3e for statistics). As T cells further differentiate, they lose expression of TCF1 although transcription of the *Tcf7* gene seems to precede the loss of the TCF1 protein itself (compare to Fig. 3b). In the dLNs, a significant increase in the frequency of $TCF1^-$ tumor-specific $CD8^+$ T cells was seen in the $CD226^+$ fraction with anti-TIGIT or combination treatment; no effect was detected in $CD226^-$ cells (Fig. 2b and Extended Data Fig. 3f).

TOX is a key transcriptional regulator of exhaustion programming and differentiation toward terminal exhaustion[22,23]. Treatment with either anti-TIGIT alone or anti-TIGIT plus anti-PD-L1 markedly decreased TOX expression in $CD226^+$ but not $CD226^-gp70^+CD8^+$ T cells in dLNs, while decreased TOX expression was seen in both $CD226^+$ and $CD226^-$ fractions in tumors; FTY720 seemed to diminish the combination effect on TOX expression in some cases (Fig. 2b,c; see Extended Data Fig. 3g for statistics).

Similar pharmacodynamic effects with combination treatment were seen in the EO771 model, with combination treatment increasing the frequency of $CD8^+$ T cells in tumors, promoting CD226 expression on tumor $CD8^+$ T cells, and increasing the $TCF1^+Tim3^+$ phenotype while reducing TOX^+ frequencies (Extended Data Fig. 3h–m).

To assess the effector state of TILs responding to checkpoint blockade, we measured production of the proinflammatory effector cytokines interferon (IFN)γ and tumor necrosis factor (TNF). Single-agent anti-TIGIT and combination treatment increased dual production of IFNγ and TNF in the $CD226^+$ fraction of intratumoral $CD8^+$ T cells relative to the $CD226^-$ fraction, with FTY720 eliminating this effect, suggesting that T cells derived from the periphery might possess superior effector function (Fig. 2d,e). Assessment of cytokine

https://doi.org/10.1038/s43018-024-00870-6

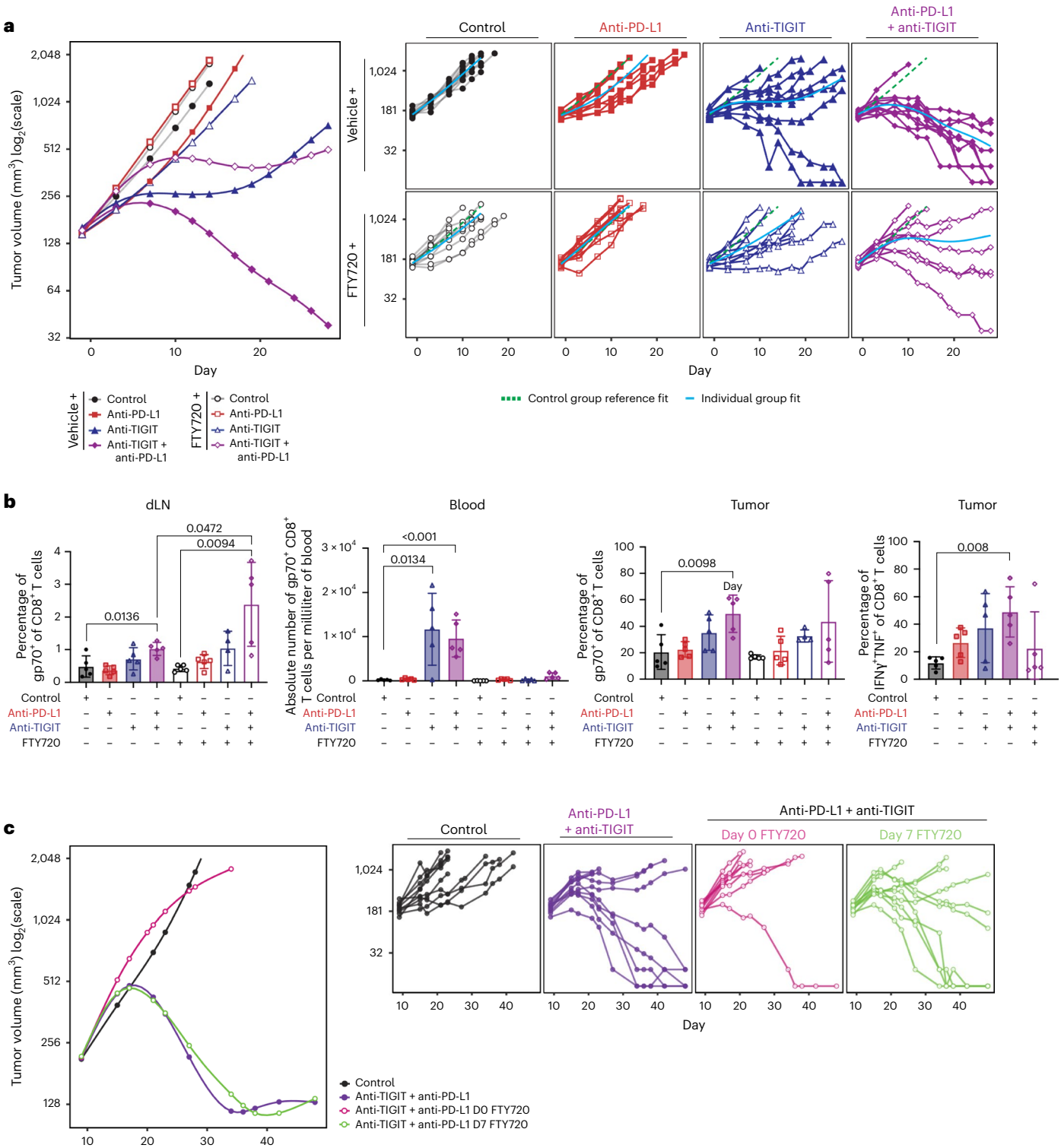

Fig. 1 | Blockade of T cell egress from dLNs reduces efficacy of anti-PD-1 and anti-TIGIT treatment in mouse CT26 tumor model. a, BALB/c mice inoculated subcutaneously with syngeneic CT26 tumor cells and treated with isotype control, anti-PD-L1, anti-TIGIT or the combination of anti-PD-L1 and anti-TIGIT antibodies, with or without FTY720. Tumor growth was monitored, and grouped analysis and growth curves for each individual animal ($n = 10$ animals per group) are shown. Tumor growth efficacy study is representative of three independent experiments. **b**, Frequency (dLN, tumor) or numbers (blood) of $CD8^+$ T cells with positive staining for the gp70-specific tetramer. Frequency of tumor $CD8^+$ T cells expressing IFNγ and TNF (right). Pharmacodynamic data are representative of three independent experiments ($n = 5$ animals per sample and treatment group). Bars represent mean; error bars represent s.d.; individual symbols represent individual animals. *P* values are indicated where differences between two groups were determined by two-way unpaired Student's *t*-test to be statistically significant. **c**, FTY720 treatment after $CD8^+$ T cells have egressed from dLNs and trafficked to tumors does not affect anti-TIGIT and anti-PD-L1 combination efficacy. FTY720 was administered on day 0, 1 day before initiation of therapy, or on day 7 after 1 week of therapy. Tumor growth was monitored, and grouped analysis and growth curves for each individual animal ($n = 10$ animals per group) are shown. Tumor growth efficacy study is representative of three independent experiments.

https://doi.org/10.1038/s43018-024-00870-6

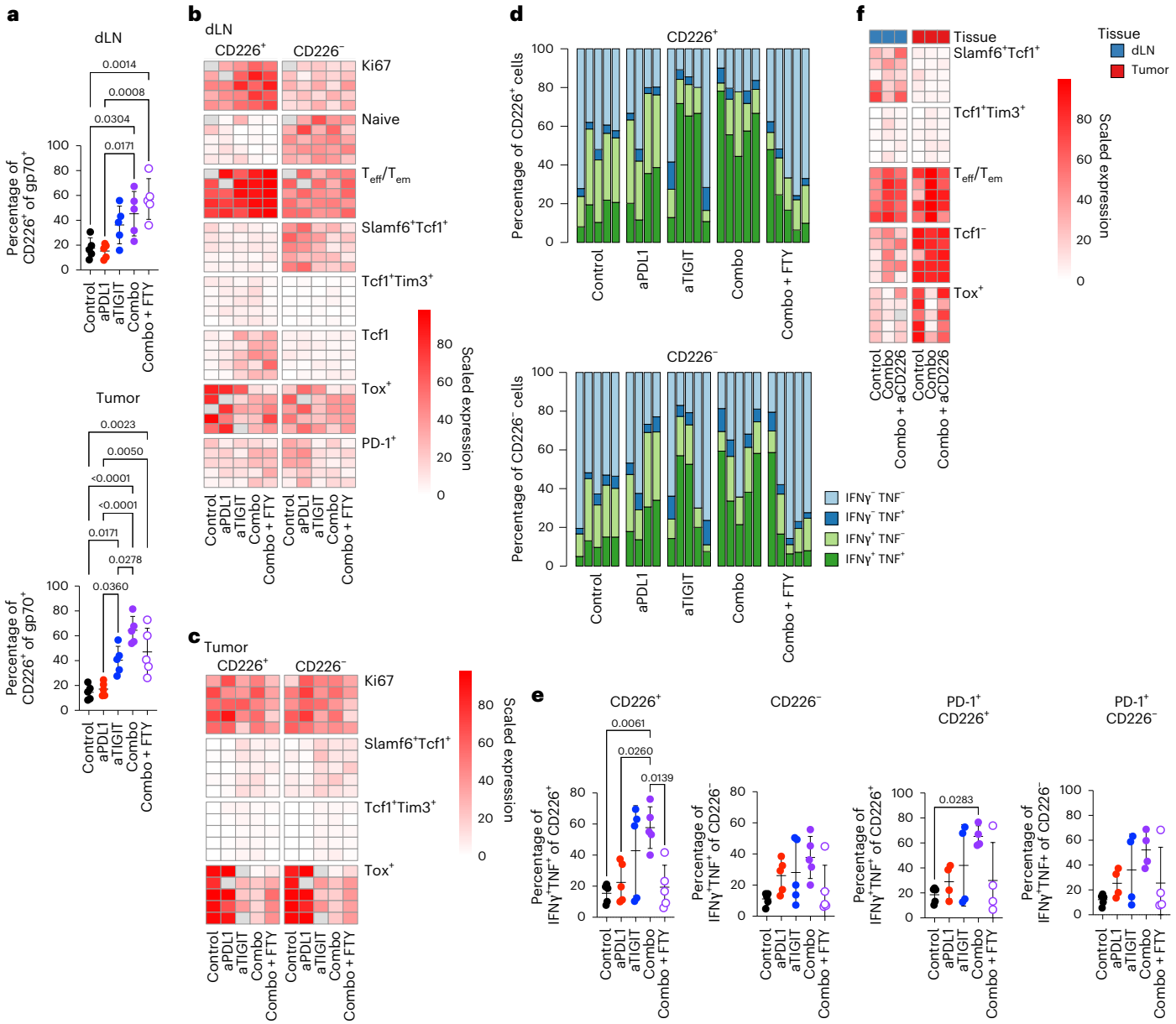

Fig. 2 | CD226 expression is a determinant of tumor-specific CD8⁺ T cell differentiation state. a, Fractions of gp70⁺CD8⁺ T cells expressing CD226 from dLNs (top) and tumors (bottom) of CT26 tumor-bearing mice treated with anti-PD-L1, anti-TIGIT or a combination with or without FTY720. **b**,**c**, Proportions of gp70⁺CD8⁺ T cells in dLNs (**b**) or tumors (**c**) having various biomarkers, separated by CD226⁺ (left) or CD226⁻ (right) status, specifically, Ki67, naive phenotype, T_{eff}/T_{em} phenotype, Slamf6 and TCF1 coexpression, TCF1 and Tim3 coexpression, nonexpression of TCF1, or TOX expression. Each row represents an individual mouse. **d**, Frequencies of CD226⁺ (top) and CD226⁻ (bottom) TILs expressing combinations of IFNγ and TNF. **e**, Individual data and statistics for fractions of IFNγ⁺ TNF⁺ cells in CD226⁺ (left) and CD226⁻ (right) bulk or PD-1⁺ TILs. **f**, Proportions of gp70⁺CD8⁺ T cells in dLNs (left) and tumor (right) having various biomarkers, under control and combination treatment, without and with anti-CD226 treatment. Data shown in **a** and **e** are represented as mean ± s.d. with individual symbols representing individual mice ($n = 5$ animals per treatment group), and are representative of three independent experiments. *P* values are indicated where differences between two groups were determined to be statistically significant by ordinary one-way ANOVA with Tukey's multiple comparisons test.

production by tumor-specific TILs was not possible due to downregulation of TCR upon in vitro stimulation; the effects were observed in PD-1⁺ TILs, indicating that activated or antigen-experienced TILs may be functionally impacted by combination treatment (Fig. 2e).

As anti-TIGIT plus anti-PD-L1 seemed to have more pronounced effects on CD8⁺ T cells expressing CD226, particularly in dLNs, we concurrently treated mice receiving the combination with CD226-blocking monoclonal antibody. As we could not segregate gp70-specific CD8⁺ T cells on the basis of CD226 expression in the presence of the blocking monoclonal antibody, we examined total gp70⁺ cells and could not discern effects on Slamf6⁺TCF1⁺ cells (Fig. 2f and Extended Data Fig. 3n); however, anti-CD226 monoclonal antibody impaired the ability of combination treatment to increase the frequency of TCF1⁺Tim3⁺ tumor-specific CD8⁺ T cells in dLNs and tumors (Fig. 2f and Extended Data Fig. 3o). CD226 blockade also showed a trend toward reducing the ability of combination treatment to drive differentiation to a T_{eff}/T_{em} phenotype (Fig. 2f and Extended Data Fig. 3p). Anti-CD226 monoclonal antibody prevented the reduction in TOX-expressing cells in dLNs and to a greater extent in tumors (Fig. 2f and Extended Data Fig. 3q; $P = 0.025$ and 0.009 respectively).

https://doi.org/10.1038/s43018-024-00870-6

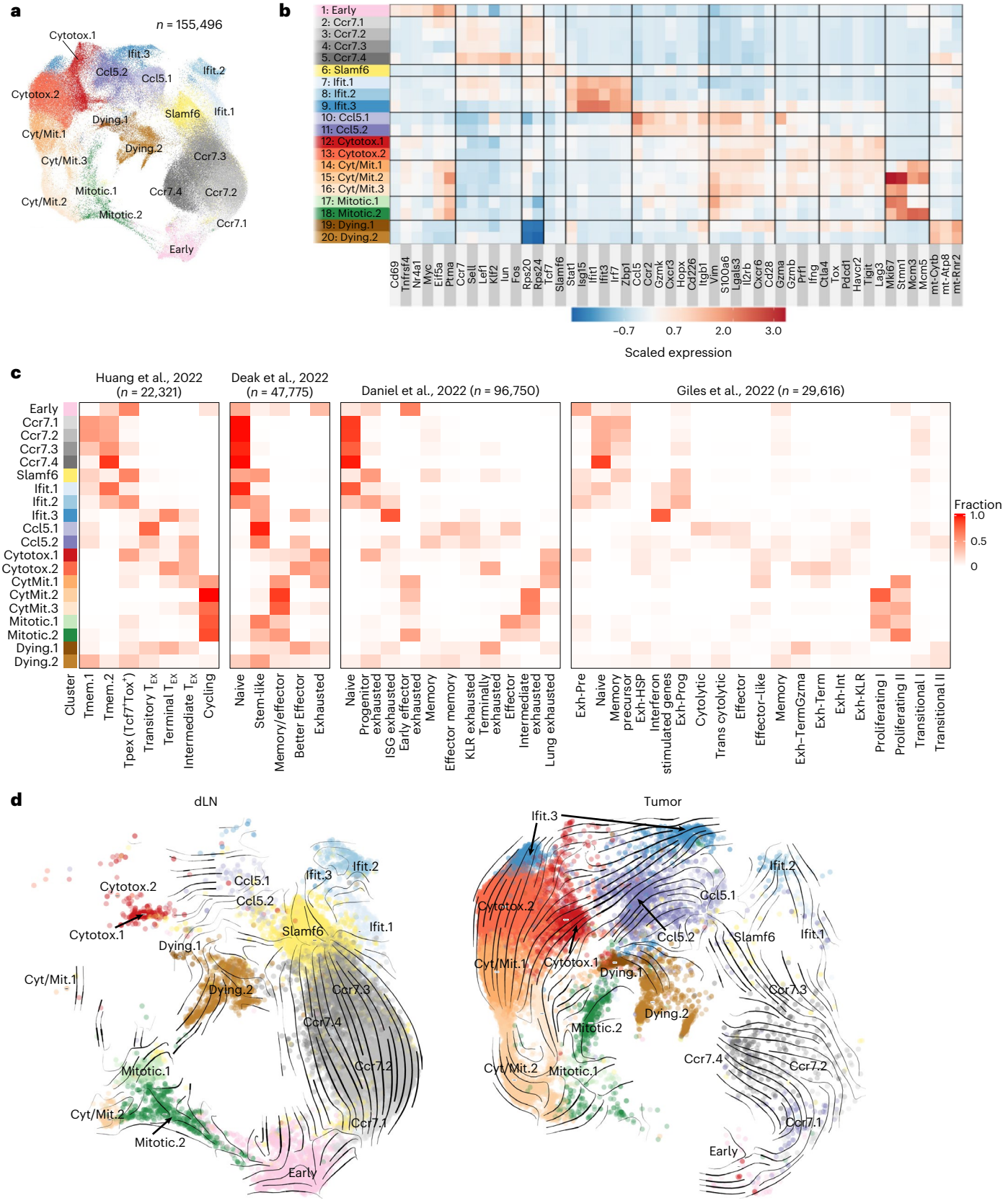

Fig. 3 | Single-cell RNA sequencing identifies distinct CD8⁺ T cell clusters in CT26 tumors, dLNs and blood. a, UMAP of 155,496 CD8⁺ T cells colored by cluster. The UMAP includes CD8⁺ T cells from all tissues. **b**, Heatmap of relative average expression of selected marker genes associated with CD8⁺ T cell phenotype, function or differentiation state in each cluster identified in the UMAP. **c**, CD8⁺ T cell cluster correspondence with reference gene signatures. Heatmaps show cross-labeling of CD8⁺ T cell clusters (rows) to reference gene signatures (columns), taken from the analyses of Huang et al.[16], Deak et al.[27], Daniel et al.[26] and Giles et al.[28], with intensities indicating normalized frequency. **d**, RNA velocity projections on UMAP for dLNs and tumors from the control treatment group.

Taken together, addition of anti-TIGIT to PD-1–PD-L1 blockade initiated distinct differentiation pathways of T_{scm} or T_{pex} cells in dLNs in a CD226-dependent fashion. These cells were further expanded in the tumor and developed into polyfunctional effectors. Similarly, the combination prevented upregulation of TOX characteristic of T_{pex} and T_{ex} differentiation, again in a CD226-dependent manner.

TIGIT and PD-L1 co-blockade expands different CD8$^+$ T cell states

We further examined how co-blockade affects the generation, phenotype and trajectory of tumor-specific T cells using a multi-omics single-cell approach, performing single-cell RNA sequencing (scRNA-seq) and TCR sequencing (scTCR-seq) on T cells from tumors, dLNs and blood. These assays were supplemented by antibody-derived tag sequencing (ADT-seq) with tetramers against gp70 and cellular indexing of transcriptomes and epitopes (CITE-seq) using a panel of 18 cell surface proteins.

Gene expression profiles of a large dataset of 245,675 T cells yielded 24 distinct clusters (Extended Data Fig. 4a), with contributions across treatment groups (Extended Data Fig. 4b), but with some clusters appearing selectively localized to dLNs, blood or tumors (Extended Data Fig. 4c). Effector status, as indicated by granzyme B expression, was confined primarily to CD8$^+$ T cells that showed clonal expansion and high ADT counts, a measure of the number of gp70 tetramers bound (Extended Data Fig. 4d–g). CITE-seq provided a complementary characterization of T cell differentiation, effector and memory states based on surface marker expression (Extended Data Fig. 4h).

We obtained greater resolution of CD8$^+$ T cell phenotypes by reanalyzing the T cells with high *CD8a* expression. These 155,496 CD8$^+$ T cells comprise one of the largest datasets used for this type of analysis, enabling higher resolution clustering and unprecedented insight into the responses of CD8$^+$ T cells to checkpoint inhibition. Twenty distinct CD8$^+$ clusters were identified (Fig. 3a,b, Extended Data Fig. 5 and Supplementary Table 1), with contributions consistent across individual mice (Extended Data Fig. 6a), experimental groups (Extended Data Fig. 6b), and clusters associating with specific tissues. Clonal expansion and ADT counts were increased in non-Ccr7 clusters (Extended Data Fig. 6c).

The clusters exhibited various phenotypes (Fig. 3a):

(a) four Ccr7 clusters ('Ccr7.1-4') characterized by *Ccr7*, a marker expressed by naive, T_{scm} and central memory (T_{cm}) cells but low in cytotoxic CD8$^+$ T_{eff} and T_{em} cells[24], as well as genes associated with T_{scm} cells such as *Sell*, *Lef1* and *Tcf7* (ref. 18) and also high expression of ribosomal proteins;
(b) a distinct cluster ('Early') characterized by expression of *Cd69* and other markers of early T cell activation;
(c) a distinct 'Slamf6' cluster marked by high *Slamf6* and *Tcf7* expression representative of a T_{scm} population;
(d) three Ifit clusters ('Ifit.1-3') with hallmarks of interferon response genes indicating activated T cells;
(e) two Ccl5 clusters ('Ccl5.1-2') marked by this chemokine that can exert chemotactic effects on T cells and is associated with CD8$^+$ T cell infiltration into tumors[25];
(f) two Cytotox clusters ('Cytotox.1-2') exhibiting hallmarks of cytotoxic gene expression as well as genes associated with exhaustion such as *Tox* and checkpoint inhibitory checkpoint receptors;
(g) three Cyt/Mit clusters ('Cyt/Mit.1-3') that represent proliferating cytotoxic cells;
(h) two mitotic clusters ('Mitotic.1-2') expressing genes associated with mitosis but not genes associated with effector function; and
(i) two clusters representing dying cells ('Dying.1-2').

The Ccl5 clusters shared expression of a number of genes associated with the Cytotox or Cyt/Mit clusters, but lacked properties of exhaustion. CITE-seq protein analysis corroborated the categorization by gene expression (Extended Data Fig. 6d–f). Both scRNA-seq and CITE-seq showed that CD226 expression was most characteristic of Ccl5.1 T cells. CD28 showed some overlapping expression with CD226 but also marked a few distinct clusters, consistent with our previous findings for human NSCLC TILs[6] (Extended Data Fig. 6d–f). The Ccl5.1 cluster is of particular interest in that it was the only major non-naive cell state found in the blood.

Comparison of our clusters with reference gene signatures from published datasets[16,26–28] showed general concordance albeit with more granularity due to the larger sample set used here (Fig. 3c). Of relevance, our Ccl5, Ifit.3 and Cytotox clusters shared strong similarities with the 'better effectors' described by others in response to a combination of anti-PD-1 therapy with interleukin (IL)-2 agonists[27]; however, our Ccl5.1 cluster also corresponded with the 'Stem-like cluster' in that study and with the 'Transitory T_{ex} cluster' by Huang and colleagues[16].

We used spliced and unspliced messenger RNA counts to estimate RNA velocities and infer differentiation trajectories. Although the directionality of cell traffic often cannot be assigned confidently from velocity-based trajectories[29], visualization results from Li and colleagues using photoactivation have established the in vivo migration of T cells into and out of tumors[24]. By assigning our clusters to the Li et al. gene expression signatures (Extended Data Fig. 7a), we could ascertain directionality in our analysis. Using control-treated tumor-bearing mice as a reference, RNA velocity patterns differed between dLNs and tumors (Fig. 3d). In dLNs, a major trajectory originated from Early and Ccr7 clusters and yielded Slamf6 cells, which then differentiated into Ifit or Ccl5 cells. In tumors, differentiation progressed from Ccl5 cells through Cytotox cells to Cyt/Mit cells. From there, a second differentiation pathway generated mitotic cells. RNA velocity patterns were similar across treatment groups, indicating that differentiation pathways were not fundamentally affected by the various treatments (Extended Data Fig. 7b,c).

Combination treatment expands Ccl5$^+$ tumor-specific CD8$^+$ T cells

We then applied our scTCR-seq data to characterize T cells by the expansion of their parent clone, which revealed notable differences across treatment groups, especially when using ADT-seq counts to distinguish gp70$^+$ from gp70$^-$ cells (Extended Data Fig. 6c). As shown in Fig. 4, cells in dLNs were predominantly singletons (having only one cell expressing a given TCR clonotype) across each cluster, but showed evidence of clonal expansion in the Slamf6 and Ccl5.1 clusters following combination treatment. In contrast, cells in tumor were almost exclusively expanded clones. Although clones were specific to individual mice, these results were not attributable to any single mouse (Extended Data Fig. 8).

On day 0 and 7, T cells in the blood across all treatment groups were largely gp70$^-$ (Fig. 4, bars facing left) and mostly in the immature Ccr7 clusters. In contrast, gp70$^+$ T cells in blood (Fig. 4, bars facing right) appeared only on day 7 and were specific to the Ccl5.1 cluster and to the anti-TIGIT and combination treatments. Expanded gp70$^-$ T cells in the Ccl5.1 cluster were observed in the blood as well; these cells could represent bystanders or clones specific to tumor antigens other than gp70. Absolute cell numbers of Ccl5.1 cells in blood were low, perhaps reflecting their transient residence in blood. The appearance of nearly all T cells in blood was blocked by FTY720 treatment, indicating that continuous egress from dLNs is required to supply blood T cells. The origin of Ccl5.1 cells from dLNs was also supported by the accumulation of clonally expanded Ccl5.1 cells in dLNs with FTY720. Tumors, unlike the dLNs or blood, contained relatively large numbers of both clonally expanded gp70$^-$ and gp70$^+$ TILs in all treatment groups; however, in mice treated with both anti-PD-L1 and anti-TIGIT, this increase

https://doi.org/10.1038/s43018-024-00870-6

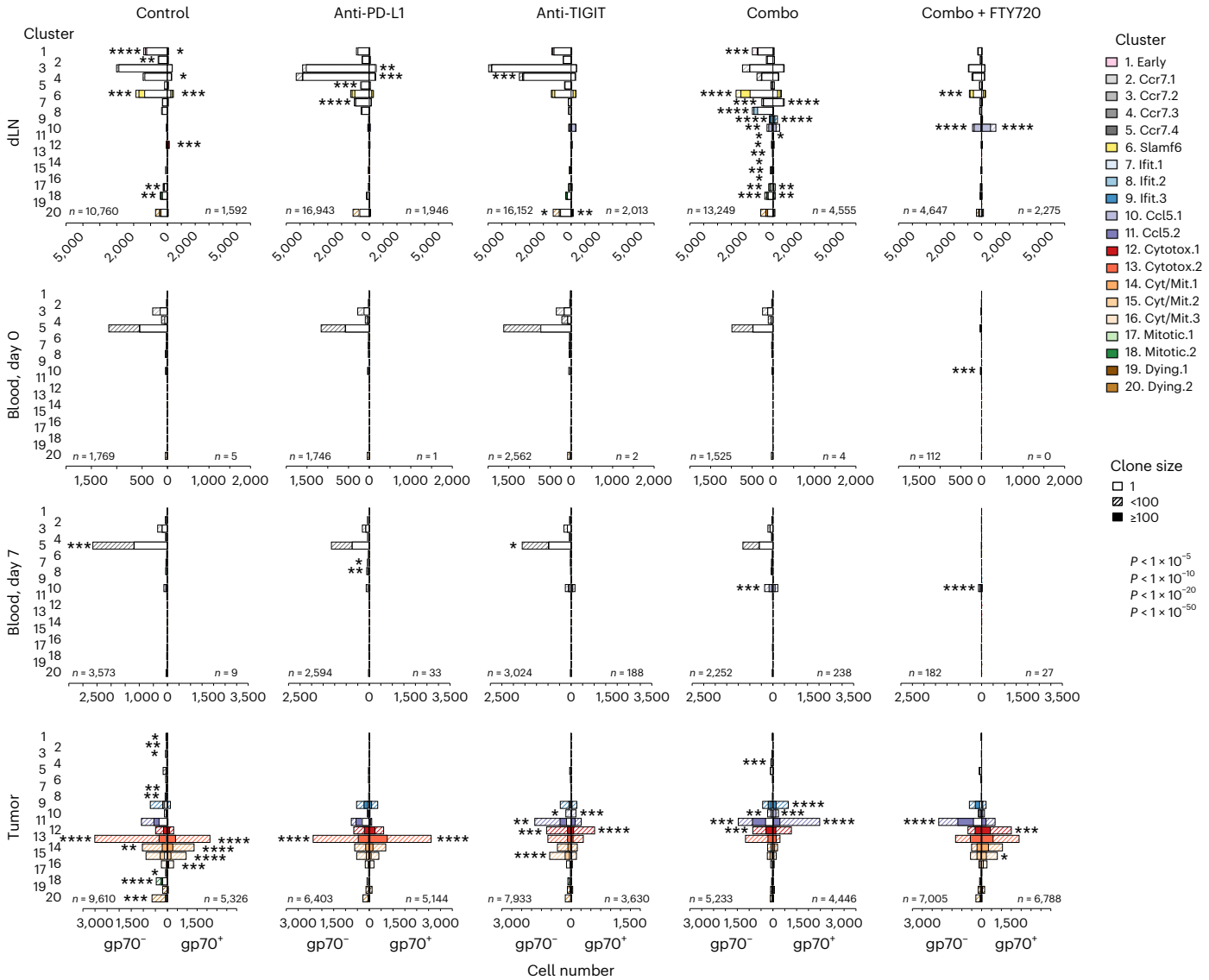

Fig. 4 | Treatment effects on CD8⁺ T cell cluster and clonal composition in CT26 tumor-bearing mice, and stacked bar graphs of CD8⁺ T cell cluster composition in each tissue under each treatment condition. Specificity for gp70 was determined by comparing ADT counts for gp70 tetramers, requiring that they should be higher than control tetramer count by a Poisson test with a one-sided *P* value < 1×10^{-6}. In each stacked bar, open bar denotes singletons, solid bar denotes numbers for clones with less than 100 cells and hatched bar denotes numbers for clones with 100 or more cells. *P* values were determined by two-sided post hoc Fisher's exact test for the indicated category relative to the rest of the contingency table and denoted by asterisks: *$P < 1 \times 10^{-5}$; **$P < 1 \times 10^{-10}$; ***$P < 1 \times 10^{-20}$; ****$P < 1 \times 10^{-50}$. *n* denotes the total number of gp70⁻ (left) or gp70⁺ (right) cells.

was relatively pronounced for gp70⁺ T cells in the Ifit and Ccl5.2 clusters (Fig. 4). The increase in gp70⁺ clones in these clusters was selectively decreased by FTY720 treatment, strongly suggesting that these cells derived proximately from the blood-borne Ccl5.1 population. In FTY720-treated mice, gp70⁺ clones expanded in the Cytotox and Cyt/Mit clusters, indicating that these may derive from pre-existing clones in tumors and expand and differentiate intratumorally in response to combined PD-L1–TIGIT blockade.

Thus, in response to combination treatment, tumor antigen-specific (and possibly also nonspecific) clonotypes expand in the dLNs, exit as Ccl5.1 cells into the blood and continue to expand after arrival in the tumor.

Co-blockade of PD-L1 and TIGIT focuses TCR clonal diversity

We next compared the degree of clonal expansion in dLNs, blood and tumors on day 7 post-treatment, characterizing each clone by its majority cluster at each site (Fig. 5a and Extended Data Fig. 9a). Inhibiting both PD-L1 and TIGIT elicited notable coordinated clonal dynamics. Although only a few clones exhibited large expansions, they did so in each of the three tissue compartments (Fig. 5a). In dLNs, expansion occurred mostly in Ifit.3 and Ccl5.1 cells, while in the tumors, Ccl5.2 cells were preferentially expanded. Combination treatment also resulted in correlated expansion in the blood (Fig. 5a, circle diameters, and Extended Data Fig. 9a). Expansion occurred with single-agent treatment (to a greater extent following anti-TIGIT alone) but was mostly limited to dLNs or tumors and not correlated between the two tissues.

In the presence of FTY720, many clones exhibited dual expansion in dLNs and tumors, but with relatively limited expansion in the blood, suggesting that these dual-expanded clones arose independently in dLNs and tumors.

The most highly expanded clones following combination treatment were gp70⁺, indicated by a high ADT count (Fig. 5b). The relatively few dual-expanded clones in the single-agent treatment groups had low or undetectable gp70 ADT counts, suggesting that they were

https://doi.org/10.1038/s43018-024-00870-6

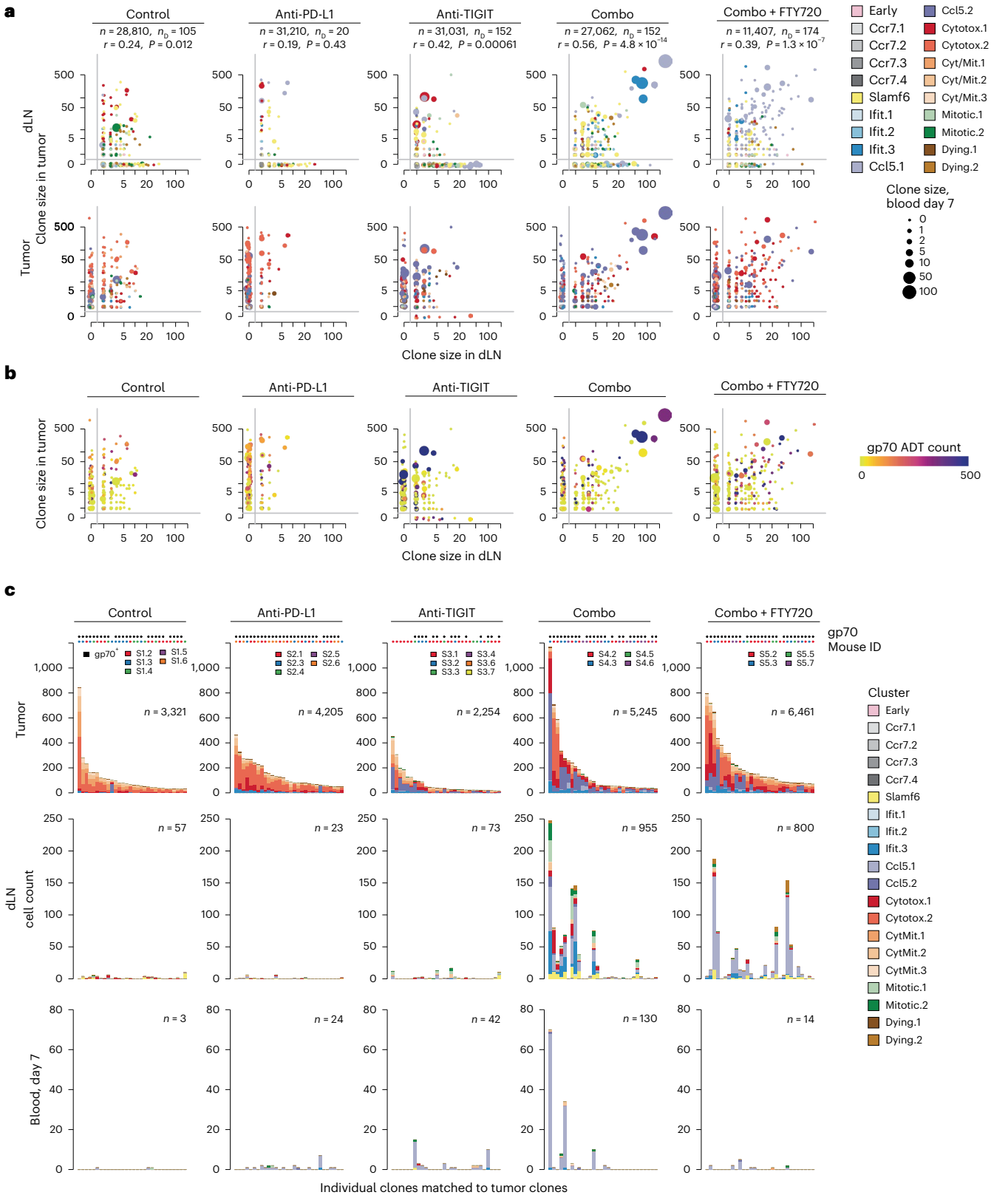

Fig. 5 | Effects of anti-PD-L1, anti-TIGIT and combination treatment on clonal diversity and dual expansion in dLNs and tumors. a,**b**, Scatter plots showing primary clusters of each individual clonotype in dLNs (top) or tumors (bottom) (**a**) or gp70 specificity and ADT count for individual clones (**b**). Color of circles denote cluster designation. Size of circles is representative of clonotype numbers detected in blood on day 7. *n* denotes the total number of clones, including those present only in dLNs or tumors; n_D refers to the number of dual clones (clones that are present in both dLNs and tumors) (**a**,**b**). *P* values were computed using a *t*-test on the Pearson correlation coefficient. **c**, Cluster composition of the top 30 largest clones in tumor with matching clonotypes, based on identical TCR usage in dLNs and blood, in absolute numbers. Clonotypes from individual mice within each treatment group are identified by the color legend at the top of the tumor bar graphs. Individual mice are labeled as S 'group number'.'mouse number'. gp70$^+$ clones are identified by a black symbol at the top of the bar graphs. Data show that all mice have clonotypes represented in the top 30 largest clones in tumor. *n* denotes the number of cells that comprise the top 30 clones (**c**).

either 'bystander' nontumor-reactive T clones[25,30] or specific for other tumor-associated antigens. In the presence of FTY720, high gp70 ADT counts were also detectable in some dual-expanded clones, as expected if these cells represented pre-existing clones already present in dLNs and tumors before treatment.

As the scatter plots (Fig. 5a,b) depict only the primary cluster type for each clone, we evaluated the composition of the 30 most expanded clones for each treatment group in tumors and matched them to dLNs and blood to study the distribution of individual clones across T cell clusters (Fig. 5c). The largest clones in tumors had measurable counterparts in dLNs but only following combination treatment. In dLNs, these clones consisted predominantly of the Ifit.3, Ccl5.1 and Cytotox.1 populations. The same expanded TCR clones were also found in the blood, again contained almost exclusively in the Ccl5.1 population. FTY720 treatment prevented the appearance of this population.

The picture was quite different with single-agent treatments. $CD8^+$ T cells in the tumor following anti-PD-L1 had largely the same composition as the control group, comprised primarily of Cytotox.2 and Cyt/Mit clusters. Expansion of the Cytotox.2 cluster was more pronounced than with other treatments, suggesting that anti-PD-L1 drives T cell differentiation toward this specific state in tumors. Anti-TIGIT, in contrast, promoted a shift in the tumor toward the Ccl5.2 cluster. With single-agent treatment, none of the largest clones in tumor had appreciable counterparts in dLNs or blood.

When we examined clonal expansion separately in each tissue compartment, each treatment had distinct effects on T cell differentiation (Extended Data Fig. 9b,c). In dLNs, anti-TIGIT and combination treatment, but not anti-PD-L1 alone, caused expansion of Ccl5.1 T cells and, to a lesser extent, Mitotic clusters. FTY720 treatment shifted the intralymphatic composition to almost exclusively Ccl5.1, suggesting that these cells accumulated in dLNs as their egress into blood was inhibited. Combination treatment, with or without FTY720, resulted in reduced proportions of the Slamf6 cluster in dLNs, especially in the most expanded clones, suggesting that the Slamf6 (putative T_{scm}) cluster might be the source from which Ccl5.1 T cells are mobilized.

Anti-PD-L1 and anti-TIGIT differentially reshape $CD8^+$ T cell trajectories

We next probed the lineage relationships across $CD8^+$ T cell clusters following various treatments. Although we previously generated cellular trajectories using RNA velocity (Fig. 3d), it is apparent that individual clones exhibit complex and distinct expansion behaviors. scTCR-seq unambiguously identifies lineages of T cells, which provides a complementary approach to infer kinetics and differentiation based on the co-occurrence of phenotypes in individual clonotypes within and across tissue compartments. We analyzed co-occurrences of cell phenotypes by tabulating numbers of intraclonal pairs over all clonotypes, plotting only pairs between different clusters (Fig. 6a–c), and interpreting such co-occurrences as steps in differentiation.

In dLNs (Fig. 6a), control mice exhibited a predominant differentiation of Slamf6 to the Cytotox.1 phenotype, with little connection to other populations as illustrated by the absence of additional intercluster links. With single-agent treatment, increased differentiation from Slamf6 to the Ccl5.1 phenotype was observed, but with anti-TIGIT further increased differentiation of Ccl5.1 cells into Cytotox.1 and Mitotic.1 cells. Combination treatment produced an even more complex pattern of differentiation, with Ccl5.1 cells also differentiating to Ifit.3 cells, and those co-occurrences being shared across cytotoxic and mitotic clusters. FTY720 treatment resulted in most Slamf6 cells differentiating to Ccl5.1, but then a sharp reduction in Ccl5.1 cells differentiating to other clusters, as indicated by the absence of intercluster links. Intraclonal pairs in dLNs consisted of primarily $gp70^+$ specificities across treatment groups, and some $gp70^-$ with control or single-agent treatment. Thus, although Slamf6 (T_{scm}) cells differentiated to cell states other than Ccl5.1 in dLN, only the Ccl5.1 population entered the blood, seeding tumors with new $CD8^+$ T cells.

Co-occurrence profiles were different in tumors compared to dLNs (Fig. 6b). Intraclonal pairs in control tumors showed an origin from the Cytotox.2 phenotype to the Cyt/Mit.1 and Cyt/Mit.2 phenotypes. Anti-PD-L1 had a similar pattern, but with additional co-occurrence of Cytotox.2 with the Ifit.3 and Cytotox.1 clusters. In sharp contrast, anti-TIGIT exhibited an expansion of clones with Ccl5.2 cells that differentiated to Cyt/Mit.2, Cyt/Mit.1 and Cytotox.2 cells; these clones were largely $gp70^-$ (blue lines), consistent with the largest clonotypes in that group being $gp70^-$ (Fig. 5c). Combination treatment resembled anti-TIGIT monotherapy in terms of Ccl5.2 expansion, but those Ccl5.2 cells differentiated primarily to Cytotox.1 cells. FTY720 treatment produced a complex pattern of co-occurrences among Ccl5.2, Cytotox.1, Cytotox.2, Cyt/Mit.1 and Cyt/Mit.2 clusters, revealing the extent of differentiation within tumors. In contrast with anti-TIGIT treatment, the vast majority of intraclonal pairs in tumors with combination treatment were $gp70^+$.

We then tabulated intraclonal pairs from across tissues to determine migration relationships, plotting only co-occurrences between different tissues, but otherwise showing co-occurrences between both same and different clusters (Fig. 6c). In contrast to single-agent therapy, the anti-PD-L1–TIGIT combination facilitated migration of Ccl5.1 cells from dLNs to Ccl5.2 cells in tumor, presumably through blood Ccl5.1 cells, but with co-occurrences from dLNs to blood less apparent because of its relatively low degree of clonal expansion in both compartments (Fig. 4). Co-occurrences were also seen from Ccl5.1 cells in dLNs to Cytotox.1 and Cytotox.2 clusters in tumors, but these were presumably attributable to intratumor differentiation (Fig. 6b). The co-occurrences between Ccl5.1 in dLNs and Ccl5.2 in tumors were also observed in the presence of FTY720, with an absence of blood involvement, indicating that combination treatment may act on pre-existing TILs in tumors that had progenitors remaining in the dLNs.

To visualize these differentiation and migration patterns in the context of gene expression, we projected the co-occurrence data onto

Fig. 6 | $CD8^+$ T cell cluster relationships within and across tissues of CT26 tumor-bearing mice following anti-TIGIT and/or anti-PD-L1 treatment. **a**,**b**, Chord diagrams showing numbers of intraclonal pairs between clusters in dLNs (**a**) or tumors (**b**). Intraclonal pairs count all pairwise combinations of cluster phenotypes summed over all clones. Lines are shown for all intraclonal pairs between cells with different clusters, with their thickness representing the number of pairs relative to the total number of pairs constituting the full circle. Regions around the circumference without lines represent intraclonal pairs between cells with the same cluster. Red lines denote $gp70^+$ clones; blue lines denote $gp70^-$ clones. Singleton clones do not have intraclonal pairs and are therefore not represented in this analysis. n_S represents the total number of pairwise counts within the same cluster; n_D is the pairwise counts between different clusters. **c**, Intraclonal pairs shared between dLNs, blood and tumors. Each chord diagram contains clusters from blood (Bl), dLNs and tumors, separated by gaps. Lines are shown for all intraclonal pairs between cells from different tissues. n_S is the pairwise counts within the same tissue; n_D is the pairwise counts between different tissues. **d**,**e**, Cluster co-occurrence links for $gp70^+$ (**d**) or $gp70^-$ (**e**) clones in dLNs, blood and tumors, projected onto UMAP plots. UMAP plots show the cells of the given tissue and gp70 specificity for each experimental condition. Thickness of lines denotes relative strength of co-occurrence and correlates with line thickness shown in chord diagrams, with an additional multiplier of 3 for migration links between tissues. Lines within dLNs and tumors were pruned by an MST algorithm to show primary relationships. Migration lines from dLNs to blood and from blood to tumor were not subjected to MST. N_L represents the total number of cells in dLNs; n_B is the number of cells in blood on day 7; n_T is the number of cells in tumors.

https://doi.org/10.1038/s43018-024-00870-6

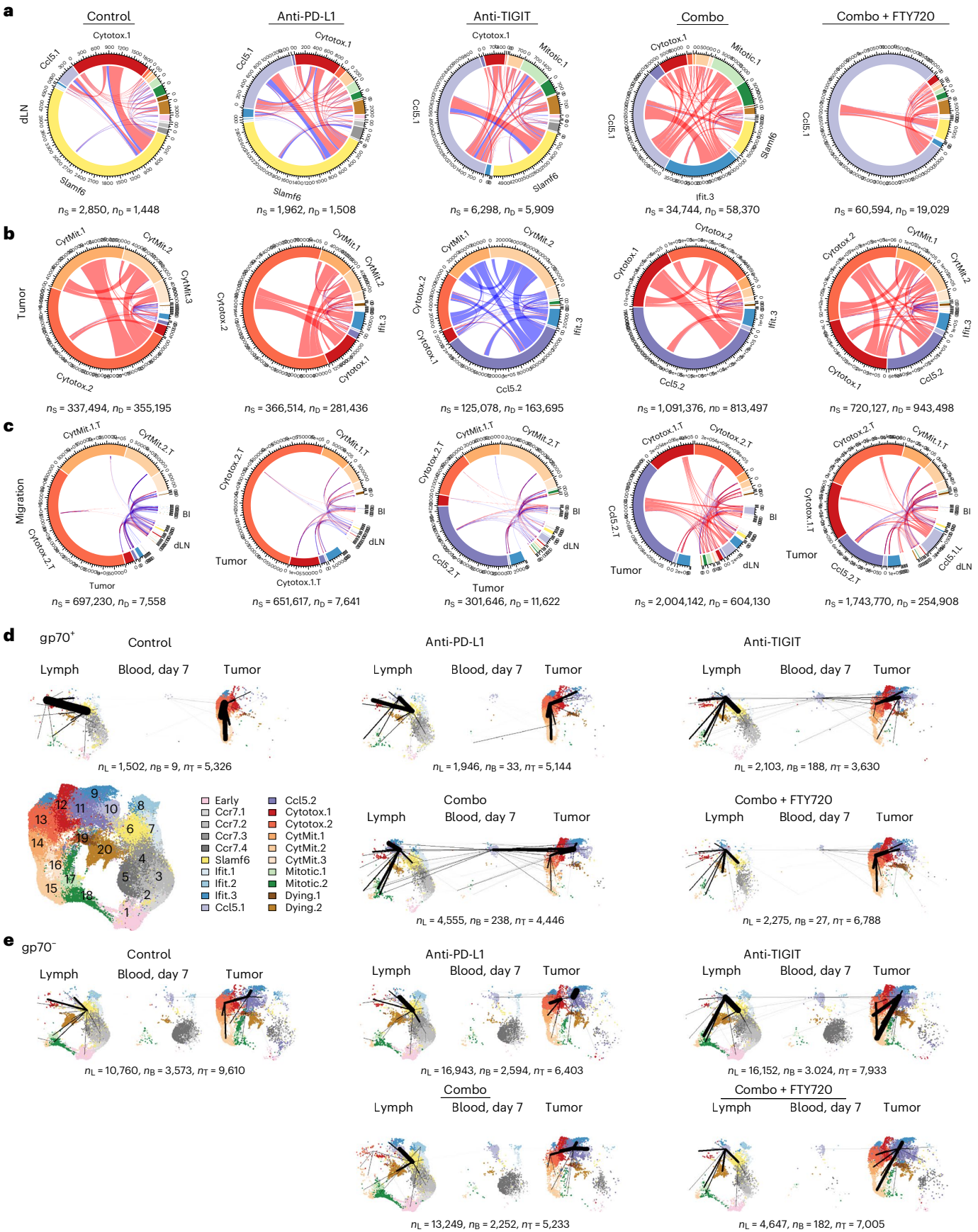

our previously computed Uniform Manifold Approximation and Projections (UMAPs). From these plots (Fig. 6d,e), it is apparent that Slamf6 cells (putative T_{scm}) in dLNs serve as progenitors for Cytotox.1 cells in control and anti-PD-L1 treated mice and for Ccl5.1 cells in other treated mice. These Ccl5.1 cells then migrate into blood, with more frequent migration occurring with anti-TIGIT and combination-treated mice in gp70$^+$ clones (Fig. 6d) than gp70$^-$ clones (Fig. 6e). In these groups, and especially with combination treatment, the migration links revealed a convergence of multiple clusters from dLNs onto Ccl5.1 cells in blood, and then a divergence from these cells into multiple clusters in tumors. With anti-TIGIT, and to a greater extent with combination therapy, gp70$^+$ Ccl5.1 cells in blood then migrated into tumor where they seemed to give rise to the Ccl5.2 phenotype. Ccl5.2 cells differentiated into Cytotox.2 cells, which then differentiated into other cytotoxic and mitotic (precursor exhausted) phenotypes. Differentiation from gp70$^+$ Cytotox.2 cells to other phenotypes was greater for anti-PD-L1 and FTY720 treatment, compared to anti-TIGIT and combination treatment. These results suggest that anti-TIGIT and especially combination treatment promote an immune response characterized by an influx of tumor-specific Ccl5.1 T cells, whereas anti-PD-L1 and FTY720 treatment exhibit primarily the differentiation of Cytotox.2 T cells already existing in the tumor.

CD8$^+$ T cell cluster association with response to tiragolumab plus atezolizumab

To explore whether these observations inform the clinical setting, we analyzed scRNA-seq data of peripheral blood T cells from a phase 1b study of patients with NSCLC treated with the combination of tiragolumab plus atezolizumab (T + A) (GO30103)[31]. We mapped human CD8$^+$ T cells onto the nearest mouse reference CD8$^+$ T cell cluster (Extended Data Fig. 10a,b). Patients with a clinical response, evaluated as either complete response (CR) or partial response (PR), compared to nonresponders (stable disease (SD) or progressive disease (PD)), had an increased frequency of CD8$^+$ T cells mapping to the Ccl5.1 and Ccl5.2 clusters and a decreased frequency mapping to Ccr7.3 and Ccr7.4 clusters (Extended Data Fig. 10c), consistent with Ccl5 clusters in our mouse models predominating with effective treatment.

To address whether gene signatures derived from the mouse CD8$^+$ T cell clusters associated with improved overall survival (OS), we analyzed bulk RNA sequencing (RNA-seq) data from baseline tumor samples from patients in CITYSCAPE[3]. The top 20 differentially expressed signature genes for each mouse CD8$^+$ T cell cluster were used to derive orthologous human gene signature 'scores' in CITYSCAPE samples (Supplementary Table 2), which compared patients treated with T + A or placebo plus atezolizumab (P + A). Ccr7.3, Slamf6, Ifit.1, Ifit.2, Ifit.3, Ccl5.2 and Cytotox.2 gene signature scores were significantly higher in CR and PR responders compared to SD and PD nonresponders (Fig. 7a). While all CD8$^+$ T cell cluster signatures trended with favorable OS hazard ratios (HRs) in patients treated with T + A compared to P + A (Extended Data Fig. 10d), high expression of Ccr7.3, Slamf6 and Ccl5.1 gene scores associated with significantly improved HRs for OS (HR 0.44 (95% CI 0.22–0.91; $P = 0.028$), 0.46 (95% CI 0.22–0.95; $P = 0.036$) and 0.45 (95% CI 0.22–0.90; $P = 0.025$), respectively), as did low expression of Cytotox.1 and Cyt/Mit.2 (OS HR 0.46 (95% CI 0.23–0.90; $P = 0.023$) and HR 0.48 (95% CI 0.23–0.98; $P = 0.045$), respectively). Dichotomization of patients on the basis of high or low cluster gene signature score and by treatment showed that high expression of the Ccl5.2 gene signature trended with increased OS with T + A but not P + A (Extended Data Fig. 10e).

Gene signatures predominantly associated with response to T + A were characterized by high expression of chemokines or chemokine receptors. We focused on *CXCR3*, *CXCR6* and *CCL5*, genes that were among the most highly expressed in each of the clusters. High expression of each of these individual genes was associated with response in patients treated with T + A (Fig. 7b) and high expression of *CCL5* or *CXCR3* was individually associated with favorable OS HR in T + A compared to P + A, outperforming *CD8A* (OS HR 0.32 (95% CI 0.14–0.73; $P = 0.006$), 0.41 (95% CI 0.18–0.94; $P = 0.035$) and 0.43 (95% CI 0.20–0.91; $P = 0.027$), respectively) (Fig. 7c). *CXCR3*, *CXCR6* and *CCL5* were associated with improved OS for T + A, again outperforming *CD8A* (Fig. 7d).

A composite gene signature score consisted of the average expression of *CCL5*, *CXCR3* and *CXCR6* was significantly higher ($P = 0.012$) in responder CITYSCAPE patients compared to nonresponders (Fig. 7e). A high gene signature score was associated with favorable OS HR in patients treated with T + A (HR 0.43; $P = 0.035$) compared to P + A, whereas a low signature score did not associate significantly with OS benefit (HR 0.70; $P = 0.277$) (Fig. 7f). Segregation of patients on the basis of high or low gene signature scores showed that those treated with T + A who had high gene score expression had improved OS compared to patients with a low gene signature (Fig. 7g). The composite gene signature score was also associated with improved progression-free survival and OS in the phase 3 OAK study (NCT02008227) of atezolizumab monotherapy in patients with locally advanced or metastatic previously treated NSCLC[32] (Extended Data Fig. 10f).

Thus, our analysis of patients treated with T + A largely recapitulates the findings of anti-TIGIT plus anti-PD-L1 in our mouse tumor studies, providing translational evidence that the events observed in dLNs of tumor-bearing mice may also be detected in human blood and tumors. Furthermore, our study suggests that CD8$^+$ T cell quality, as represented by newly arrived cells from dLNs, rather than the mere presence of CD8$^+$ T cells in the tumors supplied by the

Fig. 7 | Associations of human CD8$^+$ T cell clusters and gene signatures with clinical response to tiragolumab plus atezolizumab. a, Human gene signature scores in baseline tumor bulk RNA-seq samples from the phase 2 CITYSCAPE NSCLC trial. Patients, irrespective of treatment arm, were separated on the basis of clinical response (CR/PR, $n = 37$ patients; SD/PD, $n = 67$ patients). Boxplots are centered at the median, with the box boundaries set at the 25th and 75th percentiles; whiskers extend 1.5 × the interquartile range. *P* values are indicated for statistically significant differences by two-tailed *t*-test without correction for multiple comparisons. **b**, Individual human gene expression in baseline tumor bulk RNA-seq samples from CITYSCAPE patients who were treated with T + A or P + A separated on the basis of clinical response as described in **a**. Statistics were performed as described in **a**. **c**, Forest plot comparing high or low expression of indicated gene associated with OS HR in T + A ($n = 53$ patients) or P + A ($n = 51$ patients) treatment groups. Mean HR with 95% CIs, determined using a univariate Cox model and *P* values from a two-sided Wald test, are shown. **d**, KM curves showing the probability of OS in P + A or T + A treatment groups dichotomized on the basis of high or low expression of indicated gene. Number of patients in each subgroup were as follows: CD8A: P + A high, $n = 26$; P + A low, $n = 25$; T + A high, $n = 26$; T + A low, $n = 27$; CXCR6: P + A high, $n = 27$; P + A low, $n = 24$; T + A high, $n = 25$; T + A low, $n = 28$; CXCR3: P + A high, $n = 29$; P + A low, $n = 22$; T + A high, $n = 23$; T + A low, $n = 30$; CCL5: P + A high, $n = 29$; P + A low, $n = 22$; T + A high, $n = 23$; T + A low, $n = 30$. For KM plots, the *P* value is from a log-rank test with a null hypothesis that there is no difference between the groups. **e**, Gene score calculated using the average expression of the CD8 gene panel consisting of *CXCR3*, *CXCR6* and *CCL5* in tumor bulk RNA-seq samples from patients treated with T + A separated on the basis of clinical response. **f**, Forest plot comparing high or low expression of composite gene score associated with OS HR in T + A ($n = 53$ patients) or P + A ($n = 51$ patients) treatment groups. Mean HR with 95% CIs, determined using a univariate Cox model and *P* values from a two-sided Wald test, are shown. **g**, KM curves showing the probability of OS in P + A or T + A treatment groups dichotomized on the basis of high or low composite gene score. Number of patients in each subgroup were as follows: P + A high, $n = 26$; P + A low, $n = 25$; T + A high, $n = 26$; T + A low, $n = 27$. For KM plots, the *P* value is from a log-rank test with a null hypothesis that there is no difference between the groups.

https://doi.org/10.1038/s43018-024-00870-6

periphery at steady state[33], may be more predictive of response and clinical benefit.

Discussion

Despite the profound influence of checkpoint inhibitors on oncology practice and our understanding of tumor immunity, one important unknown is whether these inhibitors work primarily in dLNs or at the tumor site, and on which populations of cells. By considering T cells not only in dLNs and tumors but also in the blood, we demonstrate that PD-1 and TIGIT act to direct T cell fate at both anatomical sites, with activation, expansion and differentiation beginning in dLNs, but with final determination of progression to T_{eff} or T_{ex} cells occurring in tumors, challenging the notion that the trajectory to exhaustion is established at or near the time of priming[9,19,34].

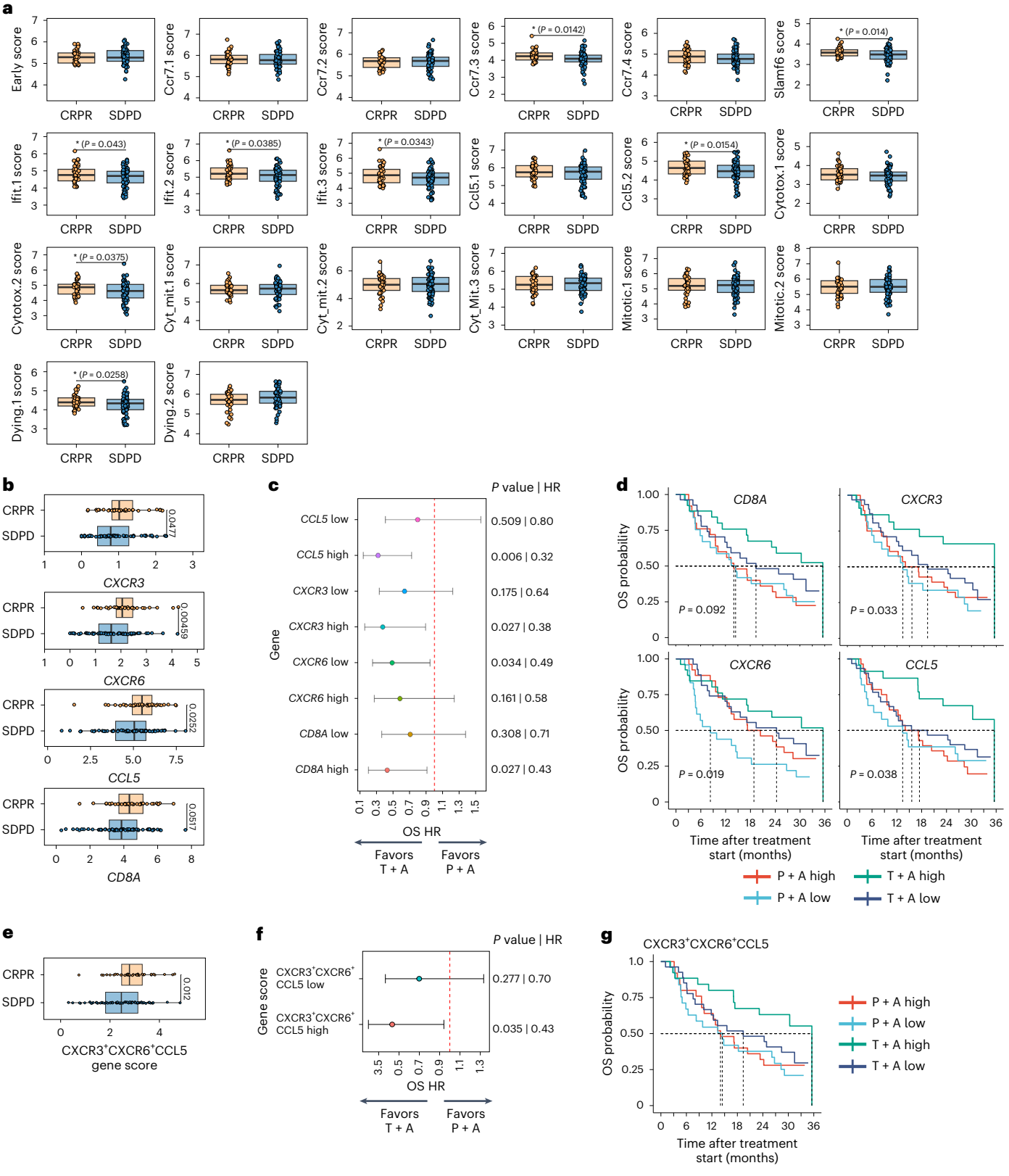

After mobilization with combination therapy, the blood compartment exhibited predominantly a single CD8$^+$ T cell population (Ccl5.1 cluster) comprising TCR clonotypes that had expanded in dLNs and that were found in the tumor. Of note, in the tumor these clonotypes were distributed among multiple T cell states. Trajectory analysis based on RNA velocity and lineage tracing of TCR clonotypes suggest that peripheral blood Ccl5.1 cells differentiated into the closely related Ccl5.2 population after reaching the tumor. Thus, polyclonal Ccl5.1 cells can be considered as 'transit cells' whose main function is to convey newly expanded T cells to the tumor.

Once in the tumor, the transit cell progeny (Ccl5.2) differentiated along the T_{ex} or T_{eff} cell pathways, a decision that seems to be influenced or determined by the degree of co-stimulation available via CD28 and CD226 co-stimulatory receptors. Indeed, CD226 signaling was required to block the expression of TOX in dLNs, and especially in the tumor where nearly 80% of tumor antigen-specific CD8$^+$ T cells were otherwise TOX$^+$. The prevention of coinhibitory receptor suppression of co-stimulatory receptor signaling by anti-PD-L1 and anti-TIGIT may explain how combination therapy directs differentiation away from the exhaustion pathway. This mechanism is consistent with observations that CD28 and CD226 signaling is under the control of the PD-1 and TIGIT coinhibitory receptors[6], thus providing an attractive functional link between checkpoint inhibition and the accumulation of T_{ex} cells in the tumor. It seems likely that dendritic cells (DCs) present in the dLNs and tumors help to determine fate decisions between T_{eff} and T_{ex} cells, as DCs present both antigen and co-stimulatory ligands, consistent with recent work[35,36]; however, the role of DCs in this proposed mechanism remains to be determined.

Notably, the effects of PD-1 and TIGIT inhibition seem to be distinct. While both facilitated the differentiation of tumor-specific T cell trajectories from the T_{scm} (Slamf6 cluster) compartment to the Ccl5.1 transit cell population in dLNs, anti-PD-L1 treatment showed differentiation also to the Cytotox.1 phenotype, whereas anti-TIGIT and combination treatment showed a second stage of extensive differentiation from the Ccl5.1 phenotype to other phenotypes. TIGIT blockade, alone or especially in combination with anti-PD-L1, produced far more emigration of tumor antigen-specific Ccl5.1 T cells into the blood than did anti-PD-L1 alone. Once in the tumor, anti-PD-L1 monotherapy showed differentiation mainly of the gp70$^+$ Ccl5.2 T cells to Cytotox.2 and then to the more exhausted Cyt/Mit phenotypes, whereas anti-TIGIT monotherapy showed differentiation mainly of the gp70$^-$ T cells also toward exhausted phenotypes. That anti-TIGIT therapy alone seemed to preferentially affect the gp70$^-$ population may be a factor in its relative therapeutic ineffectiveness. Combination therapy showed a coordinated infiltration of gp70$^+$ tumor-specific T cells from the blood and less exhaustion of T cells in the tumor, suggesting replenishment by newly arriving T cells into the tumor.

T_{scm} or T_{pex} cells have been proposed as targets for PD-1–PD-L1-targeted immunotherapies[11,14,16,17], so they are likely also targets for PD-L1–TIGIT combination. Both are presumed to be precursor populations, consistent with our results, but it is difficult to precisely map our subpopulations to these designations. Nevertheless, our scRNA-seq study has greater resolution relative to previous studies, given its large number of cells studied across a range of effective and ineffective treatments. T_{scm} cells were originally defined as a CXCR5$^+$/TCF1$^+$/Slamf6$^+$ self-renewing compartment present in dLNs that give rise to all subsequent T cells[19]. T_{pex} are generally defined as cells that have at least some of these features (Slamf6 and TCF1) and also some, but not all, features of exhausted cells; evidence indicates that they are along a continuum of precursors of terminally differentiated T_{ex} cells[18,19,34]. These two populations are often invoked interchangeably. Our evidence suggests that the anti-PD-L1–anti-TIGIT combination works on a precursor population, likely defined by our Slamf6$^+$ cluster in dLNs and subsequently the Ccl5.1 and Ccl5.2 clusters in the tumor. The effect of combination treatment, however, enables these populations to give rise to T_{eff}, not just T_{ex} cells, and it is these T_{eff} cells that seem to correlate with effective treatment. Were it possible to conduct the experiments for longer periods, it seems likely that combination treatment would also favor the differentiation of T_{em} cells in addition to T_{eff} cells. At this point, there is no single marker that unequivocally defines the Ccl5.1 or Ccl5.2 clusters, precluding experimental validation through methods such as in vivo adoptive cell transfer. Although it will ultimately be important to agree upon a common lexicon, our finding that the anti-PD-L1–anti-TIGIT combination influences CD8$^+$ T cell trajectories in a manner dependent on co-stimulatory receptor signaling can be viewed within any of the existing frameworks.

It is noteworthy that features of the T cell populations observed for combination treatment in mice seem to have counterparts in human patients with cancer who respond to combination treatment with T + A. Specifically, markers associated with Ccl5 clusters in mice, which represent newly expanded T cell clones trafficking from dLNs to tumors, were found to be associated with clinical benefit. If the differentiation trajectories influenced by blockade of PD-1–PD-L1 and TIGIT observed in mouse tumor models are also recapitulated in human patients with cancer, then more persistent and durable responses with better survival outcomes may be attained by focusing our therapeutic efforts on generating tumor-reactive effector cells that are either resistant to exhaustion programming or replacements for terminally exhausted cells. Of note, combination of PD-1 blockade with immunostimulatory cytokines such as IL-2 (refs. 27,37), blockade of immunosuppressive cytokines such as TGF-β[38] or co-stimulatory (for example 4-1BB) agonists[18] may also skew T_{scm}/T_{pex} differentiation trajectories toward effector and cytotoxic states and/or away from exhaustion. As combination of anti-TIGIT with anti-PD-L1 has the additional mechanism of action of reshaping the TME[4], higher quality antitumor T cells generated in response to combination treatment will be able to exert their effector function in a less suppressive, more permissive environment. Leveraging combination therapy strategies such as anti-TIGIT with anti-PD-L1 that drive both mechanisms may potentially bring improved clinical benefit for more patients beyond anti-PD-(L)1 alone.

Methods

Ethics statement

All experimental animal studies were conducted under the approval of the Institutional Animal Care and Use Committees (IACUCs) of Genentech Lab Animal Research and were performed in an Association for the Assessment and Accreditation of Laboratory Animal Care-accredited facility. Study design, patient cohort and response assessment for clinical trials GO30103 (NCT02794571)[31] and CITYSCAPE (NCT03563716)[3] have been previously described[4], with trial protocols approved by the institutional review board or ethics committee at each participating center and complying with Good Clinical Practice guidelines, and studies performed in accordance with the principles of the Declaration of Helsinki, the International Council for Harmonization guidelines for Good Clinical Practice and country-specific laws and regulations, as noted in the originally published clinical trials[3,31]. GO30103 (ref. 31) was conducted at 13 sites in six countries (Australia, Canada, France, South Korea, Spain and the United States). CITYSCAPE[3] was conducted in 41 clinical centers across France, Serbia, South Korea, Spain, Taiwan and the United States. All patients provided written informed consent. An internal monitoring committee reviewed available safety data periodically to make recommendations regarding study conduct to ensure the safety of patients enrolled in the study, as noted in the originally published clinical trials[3,31].

Mice

BALB/c or C57BL/6 mice were purchased from the Charles River or Jackson Laboratories. Mice were housed under specific-pathogen-free conditions at the Genentech animal facility. Mice were maintained in accordance with the Guide for the Care and Use of Laboratory Animals

(National Research Council, 2011). Genentech is an American Association of Laboratory Animal Care-accredited facility and all animal activities in this research study were conducted under protocols approved by the Genentech IACUC. Mice were housed in individually ventilated cages within animal rooms maintained under a 14 h–10 h light–dark cycle. Animal rooms were temperature and humidity controlled between 68 and 79 °F (20.0–26.1 °C) and from 30% to 70%, respectively, with 10–15 room air exchanges per hour. Female mice (aged 6–8 weeks) that seemed healthy and free from obvious abnormalities were used for the study.

Cell lines

CT26 (ATCC-CRL2638) and EO771 (ATCC-CRL3461) cell lines (obtained ATCC with corresponding certificates of analysis) were maintained at a dedicated internal cell line facility and tested to be mycoplasma free. CT26 or EO771 cells were cultured in RPMI 1640 medium supplemented with 10% FBS and 100 U ml^{-1} penicillin and 100 mg ml^{-1} streptomycin, and grown in a 37 °C humidified, 5% CO_2 incubator.

Syngeneic tumor studies

CT26 tumor studies were performed by inoculating age-matched 6–8-week-old BALB/c female mice with a subcutaneous injection of 0.1×10^6 CT26 cells in 100 µl Hank's balanced salt solution (HBSS) and Matrigel (BD Biosciences). EO771 tumor studies were performed by inoculating age-matched 6–8-week-old C57BL/6 female mice with an injection into the fifth mammary fat pad of 0.1×10^6 EO771 cells in 100 µl HBSS + Matrigel. Once tumors achieved a mean volume of 150–200 mm^3, animals were apportioned into treatment groups and treated with isotype control (anti-gp120 mIgG2a), 10 mg kg^{-1}; anti-PD-L1.mIgG2a LALAPG monoclonal antibody (clone 6E11), 10 mg kg^{-1} followed by 5 mg kg^{-1}; anti-TIGIT.mIgG2a monoclonal antibody (clone 10A7), 10 mg kg^{-1}; or TIGIT.mIgG2a.LALAPG, 10 mg kg^{-1}; and administered intravenously for the first dose and subsequently intraperitoneally. For the tracking of tumor volume, doses were given three times a week for 3 weeks. For single-cell analyses, the mIgG2a version of anti-TIGIT was used and three doses were given over the course of 1 week. To inhibit trafficking, FTY720 (Cayman Chemical Company, 1 mg kg^{-1}) was administered by daily oral gavage starting day −1 before indicated treatment, or where indicated, day 7 after treatment, and continued until end of study. Tumor volumes were measured and calculated twice per week using the modified ellipsoid formula $1/2 \times (\text{length} \times \text{width}^2)$. For pharmacodynamic analyses, mice were killed on day 7 after initial treatment. Tumors were dissociated into single-cell suspensions by using gentleMACS dissociator (Miltenyi Biotec) and enzymatically digested in a buffer containing collagenase D (2 mg ml^{-1}) and DNase (40 U ml^{-1}, Roche). Single-cell suspensions of dLNs were obtained by mechanical dissociation through 40-µm cell strainers and performing red blood cell lysis as needed. Blood was obtained by terminal cardiac puncture and collected in lavender Microtainer Blood Collection Tubes (BD Biosciences, 365974) and subjected to red blood cell lysis. Data collection and analyses from mouse tumor studies were not performed blind to the conditions of the experiment. The maximum tumor size approved by the IACUC was 2,000 mm^3. Animals bearing tumors exceeding 2,000 mm^3 or showing ulceration were killed following protocols approved by the IACUC. Tumors were measured three times per week. In the case of tumors exceeding 2,000 mm^3, tumor measurement was recorded before killing. To minimize the number of mice with tumors exceeding 2,000 mm^3, mice were killed if tumors were measured at greater than 1,700 mm^3 on any given day, as the tumor growth rate would make it highly likely for the tumor to exceed 2,000 mm^3 by the next measurement; however, despite these measures, some tumors grew in excess of 2,000 mm^3 between two measurements, as outlined here. In Fig. 1a, 8 mice were killed with tumors >1,700 mm^3, 8 mice with tumors >2,000 mm^3, 44 mice with ulcerations and 1 mouse for other reason, across the entire study. In Fig. 1c, 5 mice were killed with tumors >2,000 mm^3, 11 mice before tumors reached 2,000 mm^3 and 1 mouse with ulceration, across the entire study. Details for experimental groups and individual mice are provided in Fig. 1 Source Data. In Extended Data Fig. 1b, 34 mice were killed with tumors >1,700 mm^3, 26 mice with tumors >2,000 mm^3 and 8 mice with ulcerations, across the entire study. Details of the experimental groups and individual mice are provided in Extended Data Fig. 1 Source Data.

Flow cytometry and FACS sorting

Immune cell phenotyping by flow cytometry was performed on single-cell suspensions from mouse dLNs, tumors and blood obtained and described elsewhere. In brief, dead cells were excluded by using a fixable viability dye. Cell surface markers were stained on ice after tetramer staining. The FoxP3 nuclear staining buffer set (Invitrogen) was then performed using recommended manufacturer's instructions to detect intracellular or nuclear staining. For intracellular cytokine detection, cells with stimulated for 4 h with Cell Stimulation Cocktail (Invitrogen, 00-4970-93) at 37 °C. After stimulation, cells were stained for surface markers and intracellular factors as described above. For obtaining cells for single-cell analysis, tumors and dLNs were processed into single-cell suspensions as described elsewhere and subjected first to tetramer staining, then surface markers and CITE-seq antibodies together. Processing of blood samples on day 0 before any treatment or on day 7 were first stained with hash-tagged antibodies, then stained with surface markers. Cells were purified by fluorescence-activated cell sorting (FACS) on a Becton Dickinson FACSAria Fusion cell sorter equipped with four lasers (405 nm, 488 nm, 561 nm and 638 nm). A 70-µm nozzle running at 70 psi and 90 kHz was used as the setup for each sort session. Before gating on fluorescence, single cells were gated using forward scatter (FSC-A) and side scatter (SSC-A) (for intact cells) and SSC-W/SSC-H and FSC-W/FSC-H (to ensure that only singlets were sorted). FACS gates were drawn to include only live single cells based on calcein blue AM+ and propidium iodide (Thermo Fisher Scientific). Antibodies used for flow cytometry, cell sorting by FACS or CITE-seq are shown in Supplementary Table 3. Samples were acquired on LSR-Fortessa or BD Symphony Instruments (BD Biosciences) using FACSDiva (v.8.0.1) or Cytek Aurora using SpectroFlo (v.3.0.3) and data were analyzed using FlowJo v.10 or higher version software (Tree Star).

Single-cell RNA-seq and TCR V(D)J clonotype profiling

Processing for single-cell expression (scRNA-seq) and T cell receptor V(D)J clonotypes (scTCR-seq) was carried out using the Chromium Single Cell 5′ Library and Gel Bead kit (10x Genomics), following the manufacturer's instructions. T cells were isolated from tumors, dLNs and blood from 31 mice. Cell density and viability from each mouse tissue of FACS-sorted $CD90^+$ T cells from tumors and blood, or $CD90^+CD44^+$ T cells from dLNs, were determined by hemacytometer. Approximately 6,000–10,000 cells per sample were used for the reverse transcription mastermix. A total of 14 cycles of PCR amplification was performed to obtain sufficient cDNA used for both RNA-seq library generation and TCR V(D)J targeted enrichment followed by V(D)J library generation after Gel Bead-in-Emulsion reverse transcription (GEM-RT) reaction and cleanup. TCR V(D)J enrichment was carried out as per the manufacturer's user guide using a Chromium Single Cell V(D) J Enrichment kit, human T cell (10x Genomics). Libraries for RNA-seq and V(D)J were prepared following the manufacturer's user guide (10x Genomics), then profiled using a Bioanalyzer High Sensitivity DNA kit (Agilent Technologies) and quantified with Qubit (Thermo Fisher Scientific). scRNA-seq libraries were sequenced in one lane of HiSeq4000 (Illumina). scTCR V(D)J libraries were tagged with a sample barcode for multiplexed pooling with other libraries, sequenced in both lanes of a HiSeq2500 machine (Illumina) using Rapid Run mode, and then demultiplexed. All sequencing was conducted according to the manufacturer's specifications (10x Genomics). Detailed information on mice, tissue isolation and batching of samples is provided in Supplementary Table 4.

Pre-processing of single-cell data

Sequencing files from Illumina assays were run through Cell Ranger v.6.1.1 against a transcriptome derived from Ensembl v.2.2.0 for the mouse genome GRCm38. The combined matrix files from the filtered_feature_bc_matrix directory for the RNA and ADT libraries were divided into separate submatrices for each sample, based on 52,636 genes for expression, 6 tetramer barcodes for ADT counts, 24 antibody measurements for CITE-seq and 10 barcodes for multiplexing of the blood samples. Measurements corresponding to various alleles of T cell receptor genes (for example, *Trbv1* through *Trbv31*) were combined into a single gene measurement (*Trbv*). As blood samples were pooled from several mice based on an encoding scheme that used two multiplex barcodes to identify each mouse, single cells were demultiplexed using the two multiplex barcodes with the highest counts. In cases of a tie for the second-highest multiplex count (4.6% of cells), those single cells could not be assigned to a particular mouse using this method. TCR sequence data from the filtered_contig_annotations.csv files were processed using a custom script that identified clones across multiple tissues in each mouse, based on identical sets of α and β sequences. To handle the blood cells that could not be assigned using the multiplex counts, blood cells with a TCR nucleotide sequence uniquely matching a cell from lymph node or tumor of a mouse in the pool were assigned to the corresponding mouse. ADT barcodes came from 12 distinct tetramers, of which 2 had gp70 antigens and the remaining 10 had a non-gp70 antigen (C28, UV or C142). A cell was assigned to an antigen based on its ADT barcode with the highest count, and was not assigned in cases of ties.

Integration of single-cell expression data

Analysis was performed in the statistical language R v.4.2.0 and with scripts written for Perl v.5.16.3. The single-cell unique molecular identifier (UMI) count matrix for each tumor and lymph node, and each pooled blood sample, was processed using scDblFinder v.1.12.0 to identify and remove doublets, or gel beads containing more than one cell. The remaining singlet count matrices were processed using Seurat v.4.1.1 using the SCTransform function (unless specified otherwise, Seurat functions were run using default parameters). All samples were merged into a single Seurat object, then subjected to a filtering process to remove anomalous or low-quality cells, where 10,584 genes were first identified as each being present in more than 1% of all cells, and then 245,675 of the 260,391 cells were retained because more than 99% of their UMI counts were represented by these genes. Counts of mitochondrial genes were not used for filtering, as such genes are present in T cells at the end of their lifespan due to apoptosis, and not necessarily an indicator of poor-quality cells.

Since the mice in this study were taken from batches on two different dates, we performed batch correction was performed using the Harmony package v.0.1.1 with the batch date as the controlling variable. We calculated principal-component analysis (PCA) cell embeddings following the procedure at https://cran.r-project.org/web/packages/harmony/vignettes/Seurat.html, where we processed the count matrix with the Seurat procedures NormalizeData; FindVariableFeatures using selection.method = 'vst' and nfeatures = 2,000; ScaleData and RunPCA on the variable genes with npcs = 30. The dataset was then processed with the procedure RunHarmony and the Seurat procedures RunUMAP and FindNeighbors on the Harmony reduction, and FindClusters to obtain 24 clusters of $CD4^+$ and $CD8^+$ T cell subtypes.

The reason that we made two calls to SCTransform is as follows. The first call was performed on individual samples before integrating them, a standard practice in Seurat protocols. The second call was required because we used Harmony, which excels at batch correction, rather than the Seurat integration procedure. Harmony requires a PCA, and this in turn requires finding variable genes and scaling the data, as described above. While SCTransform is essentially equivalent to NormalizeData, FindVariableGenes and ScaleData, we used these three steps separately as this is a recommended procedure for Harmony. Furthermore, we used the procedure FindVariableFeatures with the parameter selection.method = 'vst' because this is recommended in the above-referenced website and the SCTransform method does not allow for this option.

Isolation of CD8 expression data

To obtain better resolution and a clustering that was not affected by the $CD4^+$ T cells, we determined the mean Cd4 and Cd8a expression of the 24 clusters, and isolated the 155,496 single cells belonging to the 16 clusters where Cd8a expression was predominant (Extended Data Fig. 4d). We then performed a re-clustering of that data using the Harmony reduction to yield 20 phenotypic $CD8^+$ clusters, which represented a reformulation of the original clusters.

Correspondences with clusters from external single-cell datasets

For each correspondence with an external dataset, we obtained metadata containing cluster assignments and scRNA-seq data for constructing centroids for each cluster. Metadata was obtained either publicly or from personal communication with the authors. In the latter case, these metadata files are provided in the software package for this paper, as mentioned in Data Availability.

For Huang et al.[16], we used metadata provided by the authors to us and scRNA-seq count data for the six samples referenced in the metadata from the NCBI Gene Expression Omnibus (GEO) for GSE180095, GSE122712, GSE152628 and GSE182509. For Daniel et al.[26], we used metadata from supplementary files and the scRNA-seq count data, both available at NCBI GEO for GSE188666. For Deak et al.[27], we used metadata provided by the authors to us, and scRNA-seq count data available at ArrayExpress for E-MTAB-11773. For Giles et al.[28], we used metadata from the Seurat object through the link provided in their paper under Data Availability and scRNA-seq count data available at NCBI GEO for GSE199563. For Li et al.[24], we used metadata (taking cluster assignments for celltype_cluster-2) and scRNA-seq normalized data from the Scanpy object available at ArrayExpress for E-MTAB-10176.

For datasets where raw counts were available, we generated normalized data by dividing each count by the total count for the cell and multiplying by 1 million to yield a value in transcripts per million (TPM) and adding 1 as a pseudo count. For GSE182509 within the analysis for Huang et al.[16], where only processed data are provided, we reversed the authors' square-root transformation and confirmed that the sum of those values for cells totaled 1,000, so that our normalization procedure would work. In that analysis, where samples came from different sources, normalization was performed before samples were limited to those genes in common across all datasets. For Li et al.[24], where only log-normalized data were available, we used that data. Then for cells belonging to each cluster, we generated a centroid for that cluster by computing a trimmed mean of the TPM for each gene, rejecting 10% of measurements from each end of the range. For datasets with raw counts, we converted centroids to a log scale by taking the logarithm base 2. These centroids were used as reference gene signatures to assign each cell from our dataset, where genes with zero expression across an entire sample were excluded, gene expression for each cell was converted to $\log_2(\text{TPM} + 1)$ and assignment was performed by the SingleR package in R, using default parameters. Assignments between the two clustering schemes were cross-tabulated and normalized by the total counts for each of our clusters.

Assignment of gp70 status

The single-cell ADT assay provided measures for each cell on its binding to two tetramers for gp70 antigens and ten for non-gp70 antigens (two for C28, five for UV and three for C142). To determine whether a cell was $gp70^+$, we used the minimum value for the gp70 as a test statistic in a Poisson test where base rate was the maximum value for the non-gp70

antigens, using the poisson.test function in R. A cell was considered gp70$^+$ if the one-sided P value with alt = 'greater' was less the 1×10^{-6}. A clone was considered gp70$^+$ if any of its cells was gp70$^+$.

Clonal co-occurrence analysis

Co-occurrence matrices were tabulated by summing intraclonal pairs across all clones. Specifically, for a given set of samples, each clone with n cells, where $n > 1$, contributed to the co-occurrence matrix with its outer product xxT, where the outer product represents the count of any two cluster–tissue pairs occurring in the same clone. For migration analysis, we performed the same computation, including all dLNs, blood day 7 and tumor samples for each experimental group and keeping track of intraclonal pairs for each combination of cluster and tissue. The resulting co-occurrence matrices were plotted using the chordDiagram function from the circlize package[39], v.0.4.15, in R, with the parameters transparency = 0.2 and reduce = 0. In the resulting plots, link widths are normalized by the total number of intraclonal pairs, which make up a full circumference. Same-cluster links or same-tissue links for the migration analysis, were hidden using the link.visible parameter.

In this co-occurrence analysis, clones contribute information according to their possible pairwise counts, so that singleton clones contribute no information and expanded clones contribute information according to the square of their size. For migration analysis in Fig. 6c, chord thicknesses are proportional to the square of the clone sizes between tissues. As effective clones are highly expanded in tumors but less expanded in dLNs and blood, lines may not be discernible between dLNs and blood while reasonable line thicknesses will be seen between blood and tumors or dLNs and tumors. We also characterized a clone as being gp70$^+$ if any one of its cells was determined to be gp70$^+$, although the largest clones also biased these counts according to the square of their size.

When projecting co-occurrence onto the UMAPs, such projections can be noisy because of the transitive nature of co-occurrence, where co-occurrence of cluster A and B and co-occurrence of clusters B and C necessarily implies co-occurrence of A and C. Therefore, to identify primary differentiation pathways, we applied a minimum spanning tree (MST) algorithm in R to the co-occurrence data within dLNs and within tumors, where links were processed in order from the largest to smallest count of intraclonal pairs, and retaining links only if they did not create a cycle in the graph with links previously kept. Co-occurrence links were plotted with the same relative thicknesses as shown in the circular co-occurrence plots of Fig. 6a–c, normalized to the total number of intraclonal pairs, but with a relative multiplier of 3 for the migration links, as they are relatively sparse.

RNA velocity analysis

The paired-end FASTQ files from each sample were mapped using kallisto bustools (v.0.46.1) to a transcriptome index from Ensembl v.90 on genome GRCm38. The transcriptome index was generated using kallisto with a read length of 90 nt and intronic sequences from BUSpaRse[40] (BUSpaRse: kallisto | bustools R utilities; R package v.1.6.1, https://github.com/BUStools/BUSpaRse). The resulting spliced and unspliced count matrices for each tissue sample from each mouse were filtered to correspond to the cells used in the Seurat-based analysis, and the Seurat-based UMAP coordinates for those cells were added to the data object. The cells for each tissue and experimental group were combined using the concatenate procedure with join = 'outer'. The resulting object was processed by scvelo package v.0.2.4 within Python v.3.7.3, using the commands 'pp.filter_and_normalize', 'pp.moments', 'tl.recover_dynamics' and 'tl.velocity' with mode = 'dynamical'. Velocity graphs were generated using the command 'tl.velocity_graph' and 'pl.velocity_embedding_stream', with the parameter arrow_size = 0.001 to hide arrows, which otherwise gave directions often inconsistent with one another and with empirically determined T cell behavior.

Projection of human CD8$^+$ T cells from a Ph1b scRNA-seq dataset to a mouse reference

Human genes from the Ph1b GO30103 (NCT02794571) scRNA-seq data were first converted to their mouse orthologs using babelgene (v.22.9). Human genes without mouse orthologs or with mouse orthologs not present in the mouse scRNA-seq dataset were left unmodified without renaming. Human CD8$^+$ T cells were then separated by patient and normalized with SCTransform in Seurat (v.4.2) using the default parameters. These samples were then integrated using reference-based integration to overcome the memory limits of canonical correlation analysis integration. The second patient in the dataset was chosen at random as the integration reference. After integration, transfer anchors were identified between the query human CD8$^+$ T cell dataset and the mouse CD8$^+$ T cell reference. The MapQuery function in Seurat was used to transfer cell type labels, integrate embeddings and to project the query data onto the reference UMAP.

Gene signature scores for CITYSCAPE

The top 20 differentially expressed genes in each of the mouse CD8$^+$ T cell clusters identified from scRNA-seq were converted to their human orthologs using babelgene (v.22.9) in R (v.4.2.0). Mouse genes that did not have human orthologs or with human orthologs that were not present in the CITYSCAPE dataset were removed. The final curated table of signature genes used for analysis is shown in Supplementary Table 2.

Analysis of CITYSCAPE and OAK clinical trial data

CITYSCAPE (NCT03563716) is a phase 2 trial investigating tiragolumab with atezolizumab compared to placebo with atezolizumab in patients with locally advanced or metastatic NSCLC[3]. Patients were treated until disease progression or loss of clinical benefit. Patient tumor samples were submitted for RNA-seq and the average, log-normalized expression of the genes shown in Supplementary Table 2 or selected genes as indicated in the text was used to define gene signature scores. Objective response was categorized according to Response Evaluation Criteria in Solid Tumors (v.1.1). For Kaplan–Meier (KM) survival curves and HRs, patients in the CITYSCAPE trial were separated by treatment group and further subdivided by high or low expression of individual genes or gene signatures, where high or low is defined as greater than or equal to, or less than, the global median expression, respectively, of that gene or gene signature score. The survminer package (v.0.4.9), survival package (v.3.4-0) and R (v.4.2.0) were used to generate the KM plot. A log-rank test was used for statistical testing on the survival data. A Cox proportional hazards regression model was fit on gene or gene signature score high or low data and the HR and 95% CI for OS calculated and plotted for patients receiving tiragolumab with atezolizumab compared to patients receiving placebo with atezolizumab. Similarly, KM survival curves for progression-free survival and OS were generated for the phase 3 OAK study (NCT02008227) evaluating atezolizumab versus chemotherapy in PD-L1-positive previously treated patients with advanced or metastatic NSCLC[32].

Statistics and reproducibility

Pharmacodynamic data were analyzed using GraphPad Prism software v.9 (GraphPad). Measures between two groups were performed with a Student's t-test (two-tailed). Groups of three or more were analyzed by one-way or two-way analysis of variance (ANOVA) followed by Tukey's post-testing for multiple comparisons, as appropriate. Reproducibility of studies is indicated by the number of independent experiments provided in figure legends. Data distribution was assumed to be normal but this was not formally tested. No statistical methods were used to predetermine sample size. Sample sizes were based on previous experience[5,6] and balanced animal welfare and statistical robustness. For syngeneic mouse tumor studies,

animals whose tumors became ulcerated before progression or CR or at time of allocation into experimental groups were killed and removed from the study. For syngeneic mouse tumor studies, data collection and analysis were not performed blind to the conditions of the experiments. CITYSCAPE was a randomize, double-blinded, placebo-controlled study[3]; for data analysis; patients were separated on the basis of clinical response irrespective of treatment arm. All other statistical methods were performed as described in the figure legends corresponding to the data figure.

Reporting summary

Further information on research design is available in the Nature Portfolio Reporting Summary linked to this article.

Data availability

FASTQ files containing raw sequencing reads for the scRNA-seq, scTCR-seq, ADT-seq and CITE-seq analyses have been deposited with the NCBI Short Read Archive under accession PRJNA911822. Processed output files from Cell Ranger and metadata with cluster assignments, clonotypes and ADT assignments have been deposited with the NCBI GEO under accession code GSE220901. Raw counts and metadata for reanalyzed scRNA-seq data from GO30103 (NCT02794571)[4,31] are available from the European Genome–Phenome Archive (EGA) under accession code EGAD50000000367 and at https://github.com/cwtran/nutsch_nature_cancer_2024/. Reanalyzed datasets from the CITYSCAPE (NCT03563716)[3,4] and OAK (NCT02008227)[4,32] clinical trials can be found under EGA accession codes EGAD50000000251 and EGAD50000000368, respectively. All data relating to mouse sequencing data at NCBI Short Read Archive and NCBI GEO and pseudoanonymized clinical trial data are available without restrictions. Due to the legal requirements for data sharing, users must agree to the Data Access Agreement detailed in the EGA entries above before they can access these human datasets. Data access requests are reviewed by the Genentech DevSci Data Access Committee (devsci-dac-d@gene.com).

Reanalysis of previously published datasets generated by others and publicly available was as follows: for Huang et al.[16], we used metadata provided by the authors to us and scRNA-seq count data for the six samples referenced in the metadata from NCBI GEO for GSE180095, GSE122712, GSE152628 and GSE182509; for Daniel et al.[26], we used metadata from supplementary files and the scRNA-seq count data, both available at NCBI GEO for GSE188666; for Deak et al.[27], we used metadata provided by the authors to us, and scRNA-seq count data available at ArrayExpress for E-MTAB-11773; for Giles et al.[28], we used metadata from the Seurat object through the link (https://www.dropbox.com/scl/fo/wuwas5f1jeac3nuw46de4/ADc75QyDwGrS_7XklqP7PLY?rlkey=9wrgn38p3hherec19xxw2rrvs&e=1&st=wimjk55a&dl=0) provided in their paper under Data Availability and scRNA-seq count data available at NCBI GEO for GSE199563; for Li et al.[24], we used metadata (taking cluster assignments for celltype_cluster-2) and scRNA-seq normalized data from the Scanpy object available at ArrayExpress for E-MTAB-10176.

Source data for Figs. 1, 2a,d,e, 3b,c, 4, 5c and 6a–c and Extended Data Figs. 1b,c, 3a–q, 6a,e, 7a, 8 and 9b,c have been provided. Source data are provided with this paper. All other data supporting the findings of this study are available from the corresponding author on reasonable request.

Code availability

Computer code used to generate the single-cell analyses and figures in this paper are provided as a Supplementary File to the NCBI GEO accession code GSE220901. Code for reanalyzed datasets from the GO30103 (NCT02794571)[4,31], CITYSCAPE (NCT03563716)[3,4] and OAK (NCT02008227)[4,32] clinical trials are accessible at https://github.com/cwtran/nutsch_nature_cancer_2024/.

References

1. Mellman, I., Chen, D. S., Powles, T. & Turley, S. J. The cancer-immunity cycle: indication, genotype, and immunotype. *Immunity* **56**, 2188–2205 (2023).
2. Chiang, E. Y. & Mellman, I. TIGIT–CD226–PVR axis: advancing immune checkpoint blockade for cancer immunotherapy. *J. Immunother. Cancer* **10**, e004711 (2022).
3. Cho, B. C. et al. Tiragolumab plus atezolizumab versus placebo plus atezolizumab as a first-line treatment for PD-L1-selected non-small-cell lung cancer (CITYSCAPE): primary and follow-up analyses of a randomised, double-blind, phase 2 study. *Lancet Oncol.* **23**, 781–792 (2022).
4. Guan, X. et al. Anti-TIGIT antibody tiragolumab leverages myeloid cells and regulatory T cells to improve PD-L1 checkpoint blockade. *Nature* **627**, 646–655 (2024).
5. Johnston, R. J. et al. The immunoreceptor TIGIT regulates antitumor and antiviral CD8$^+$ T cell effector function. *Cancer Cell* **26**, 923–937 (2014).
6. Banta, K. L. et al. Mechanistic convergence of the TIGIT and PD-1 inhibitory pathways necessitates co-blockade to optimize anti-tumor CD8$^+$ T cell responses. *Immunity* **55**, 512–526 (2022).
7. Gattinoni, L. et al. A human memory T cell subset with stem cell-like properties. *Nat. Med.* **17**, 1290–1297 (2011).
8. Lugli, E., Galletti, G., Boi, S. K. & Youngblood, B. A. Stem, effector, and hybrid states of memory CD8$^+$ T cells. *Trends Immunol.* **41**, 17–28 (2020).
9. Zehn, D., Thimme, R., Lugli, E., Pereira de Almeida, G. & Oxenius, A. Stem-like precursors are the fount to sustain CD8$^+$ T cell responses. *Nat. Immunol.* **23**, 836–847 (2022).
10. Galletti, G. et al. Two subsets of stem-like CD8$^+$ memory T cell progenitors with distinct fate commitments in humans. *Nat. Immunol.* **21**, 1552–1562 (2020).
11. Siddiqui, I. et al. Intratumoral Tcf1$^+$PD-1$^+$CD8$^+$ T cells with stem-like properties promote tumor control in response to vaccination and checkpoint blockade immunotherapy. *Immunity* **50**, 195–211. e110 (2019).
12. Im, S. J. et al. Defining CD8$^+$ T cells that provide the proliferative burst after PD-1 therapy. *Nature* **537**, 417–421 (2016).
13. Kurtulus, S. et al. Checkpoint blockade immunotherapy induces dynamic changes in PD-1$^-$CD8$^+$ tumor-infiltrating T cells. *Immunity* **50**, 181–194.e186 (2019).
14. Kallies, A., Zehn, D. & Utzschneider, D. T. Precursor exhausted T cells: key to successful immunotherapy? *Nat. Rev. Immunol.* **20**, 128–136 (2020).
15. Dammeijer, F. et al. The PD-1/PD-L1-checkpoint restrains T cell immunity in tumor-draining lymph nodes. *Cancer Cell* **38**, 685–700 (2020).
16. Huang, Q. et al. The primordial differentiation of tumor-specific memory CD8$^+$ T cells as bona fide responders to PD-1/PD-L1 blockade in draining lymph nodes. *Cell* **185**, 1–18 (2022).
17. Connolly, K. A. et al. A reservoir of stem-like CD8$^+$ T cells in the tumor-draining lymph node preserves the ongoing antitumor immune response. *Sci. Immunol.* **6**, eabg7836 (2021).
18. Barboy, O. et al. Modeling T cell temporal response to cancer immunotherapy rationalizes development of combinatorial treatment protocols. *Nat. Cancer* https://doi.org/10.1038/s43018-024-00734-z (2024).
19. Giles, J. R., Globig, A.-M., Kaech, S. M. & Wherry, E. J. CD8$^+$ T cells in the cancer-immunity cycle. *Immunity* **56**, 2231–2253 (2023).
20. Pinschewer, D. D. et al. FTY720 immunosuppression impairs effector T cell peripheral homing without affecting induction, expansion, and memory. *J. Immunol.* **164**, 5761–5770 (2000).
21. Huang, A. Y. et al. The immunodominant major histocompatibility complex class I-restricted antigen of a murine colon tumor derives from an endogenous retroviral gene product. *Proc. Natl Acad. Sci. USA* **93**, 9730–9735 (1996).

22. Scott, A. C. et al. TOX is a critical regulator of tumour-specific T cell differentiation. *Nature* **571**, 270–274 (2019).
23. Khan, O. et al. TOX transcriptionally and epigenetically programs CD8$^+$ T cell exhaustion. *Nature* **571**, 211–218 (2019).
24. Li, Z. et al. In vivo labeling reveals continuous trafficking of TCF-1$^+$ T cells between tumor and lymphoid tissue. *J. Exp. Med.* **219**, e20210749 (2022).
25. Meier, S. L., Satpathy, A. T. & Wells, D. K. Bystander T cells in cancer immunology and therapy. *Nat. Cancer* **3**, 143–155 (2022).
26. Daniel, B. et al. Divergent clonal differentiation trajectories of T cell exhaustion. *Nat. Immunol.* **23**, 1614–1627 (2022).
27. Deak, L. C. et al. PD-1-*cis* IL-2R agonism yields better effectors from stem-like CD8$^+$ T cells. *Nature* https://doi.org/10.1038/s41586-022-05192-0 (2022).
28. Giles, J. R. et al. Shared and distinct biological circuits in effector, memory and exhausted CD8$^+$ T cells revealed by temporal single-cell transcriptomics and epigenetics. *Nat. Immunol.* **23**, 1600–1613 (2022).
29. Bergen, V., Soldatov, R. A., Kharchenko, P. V. & Theis, F. J. RNA velocity–current challenges and future perspectives. *Mol. Syst. Biol.* **17**, e10282 (2021).
30. Simoni, Y. et al. Bystander CD8$^+$ T cells are abundant and phenotypically distinct in human tumour infiltrates. *Nature* **557**, 575–579 (2018).
31. Kim, T. W. et al. Anti-TIGIT antibody tiragolumab alone or with atezolizumab in patients with advanced solid tumors: a phase 1a/1b nonrandominzed controlled trial. *JAMA Oncol.* **9**, 1574–1582 (2023).
32. Rittmeyer, A. et al. Atezolizumab versus docetaxel in patients with previously treated non-small-cell lung cancer (OAK): a phase 3, open-label, multicentre randomised controlled trial. *Lancet* **389**, 255–265 (2017).
33. Tumeh, P. C. et al. PD-1 blockade induces responses by inhibiting adaptive immune resistance. *Nature* **515**, 568–571 (2014).
34. Brunell, A. E., Lahesmaa, R., Autio, A. & Thotakura, A. K. Exhausted T cells hijacking the cancer-immunity cycle: assets and liabilities. *Front. Immunol.* **14**, 1151632 (2023).
35. Pittet, M. J., Di Pilato, M., Garris, C. & Mempel, T. R. Dendritic cells as shepherds of T cell immunity in cancer. *Immunity* **56**, 2218–2230 (2023).
36. Oh, S. A. et al. PD-L1 expression by dendritic cells is a key regulatory of T-cell immunity in cancer. *Nat. Cancer* **1**, 681–691 (2020).
37. Hashimoto, M. et al. PD-1 combination therapy with IL-2 modifies CD8$^+$ T cell exhaustion program. *Nature* https://doi.org/10.1038/s41586-022-05257-0 (2022).
38. Castiglioni, A. et al. Combined PD-L1/TGFβ blockade allows expansion and differentiation of stem cell-like CD8 T cells in immune excluded tumors. *Nat. Commun.* **14**, 4703 (2023).
39. Gu, Z., Gu, L., Eils, R., Schlesner, M. & Brors, B. *circlize* implements and enhances circular visualization in R. *Bioinformatics* **30**, 2811–2812 (2014).
40. Moses, L. & Pachter, L. Museum of spatial transcriptomics. *Nat. Methods* **19**, 534–546 (2022).

Acknowledgements

We thank the patients who kindly provided tumor samples for this study, as well as the investigators and staff involved in the GO30103, CITYSCAPE[3,4] and OAK studies. We thank Genentech's FACS core facility for contributing their expertise and performing cell sorting. We thank the Genentech laboratory animal core groups for microinjection, animal care and genotyping support. We thank L. Adams for providing assistance with the pharmacodynamic studies. We thank R. Johnston, J. Grogan, A. Chitre and S. Oh for thoughtful discussions.

Author contributions

K.N., K.L.B. and E.D. performed in vivo tumor studies, pharmacodynamic studies, bioinformatic studies and data analysis; T.D.W., K.W. and S. Müller performed mouse bioinformatic analyses; S. Mittman and Y.Q. managed and performed in vivo tumor studies; C.W.T., B.Y.N. and N.S.P. performed clinical trial bioinformatic analyses; K.N., K.L.B., E.Y.C. and I.M. conceived this work; E.Y.C. and I.M. supervised this work; and K.N., K.L.B., T.D.W., E.Y.C. and I.M. wrote the paper.

Competing interests

The authors declare the following competing interests: all authors are employees of Genentech, a member of the Roche group, which develops and markets drugs for profit.

Additional information

Extended data is available for this paper at https://doi.org/10.1038/s43018-024-00870-6.

Supplementary information The online version contains supplementary material available at https://doi.org/10.1038/s43018-024-00870-6.

Correspondence and requests for materials should be addressed to Eugene Y. Chiang or Ira Mellman.

Peer review information *Nature Cancer* thanks Hazem Ghoneim and the other, anonymous, reviewer(s) for their contribution to the peer review of this work.

https://doi.org/10.1038/s43018-024-00870-6

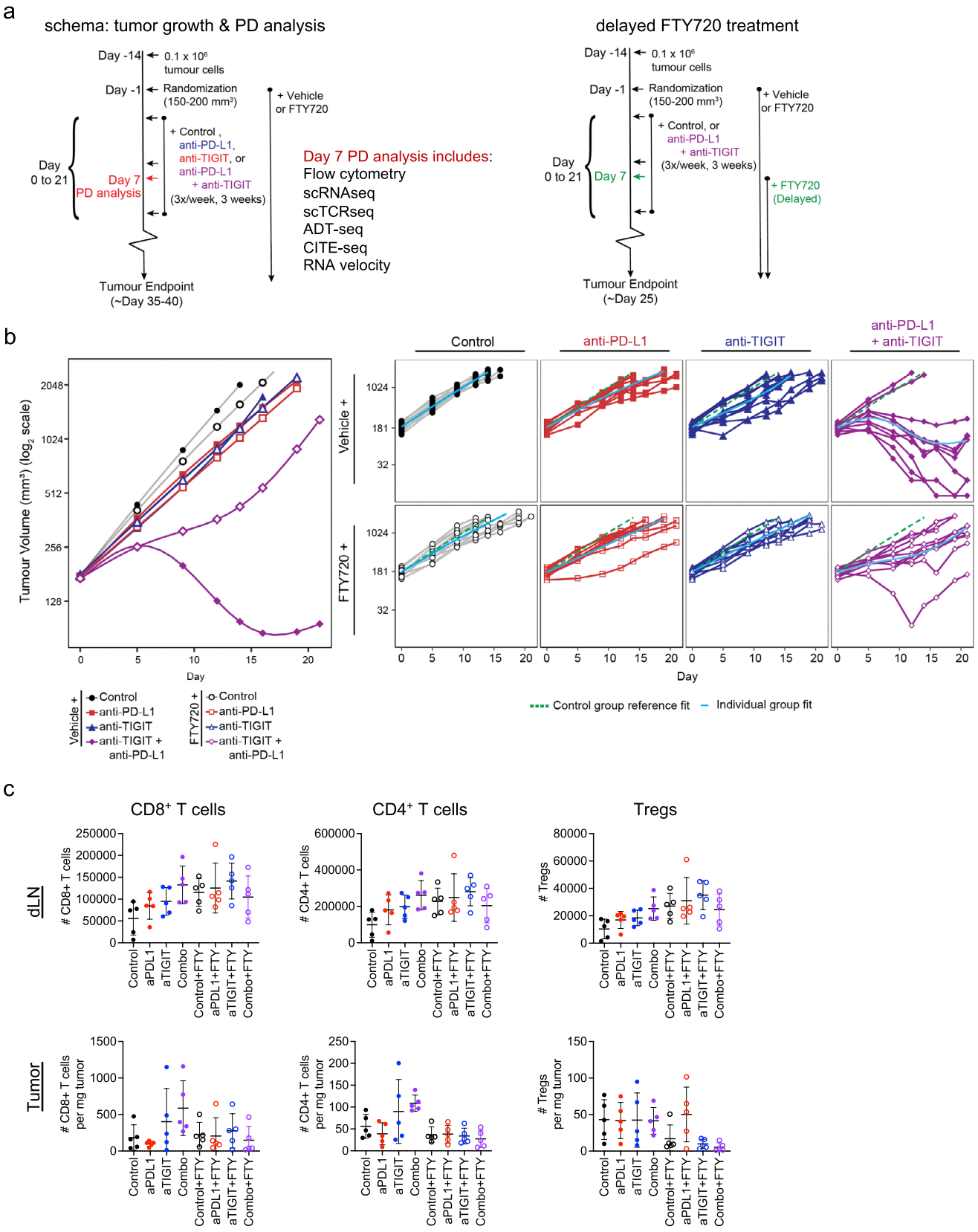

Extended Data Fig. 1 | See next page for caption.

https://doi.org/10.1038/s43018-024-00870-6

Extended Data Fig. 1 | Experimental schemas, efficacy and pharmacodynamic data for CT26 and EO771 studies. a, Experimental schemas. Tumor growth and PD/multi-omics analysis for CT26 and EO771 studies (left); delayed FTY720 treatment in CT26 model (right). **b, c**, Mouse EO771 orthotopic tumor model. **b**, FTY720 treatment impairs efficacy of anti-PD-1 and anti-TIGIT treatment in EO771 tumor model. C57BL/6 mice inoculated in mammary fat pad with EO771 tumor cells and treated with isotype control, anti-PD-L1, anti-TIGIT, or the combination of anti-PD-L1 and anti-TIGIT antibodies, with or without FTY720. Tumor growth was monitored and grouped analysis and growth curves for each individual animal are shown (n = 10 animals per group). Data shown are representative of two independent experiments. **c**, Total numbers of $CD8^+$ T cells, $CD4^+$ T cells or Tregs in dLN (top panels) or tumor (bottom panels) of CT26 tumor-bearing mice treated with isotype control, anti-PD-L1, anti-TIGIT or the combination, with or without FTY720. n = 5 animals per sample and treatment group, mean ± s.d. are represented by bars and whiskers. Data are representative of three independent experiments.

https://doi.org/10.1038/s43018-024-00870-6

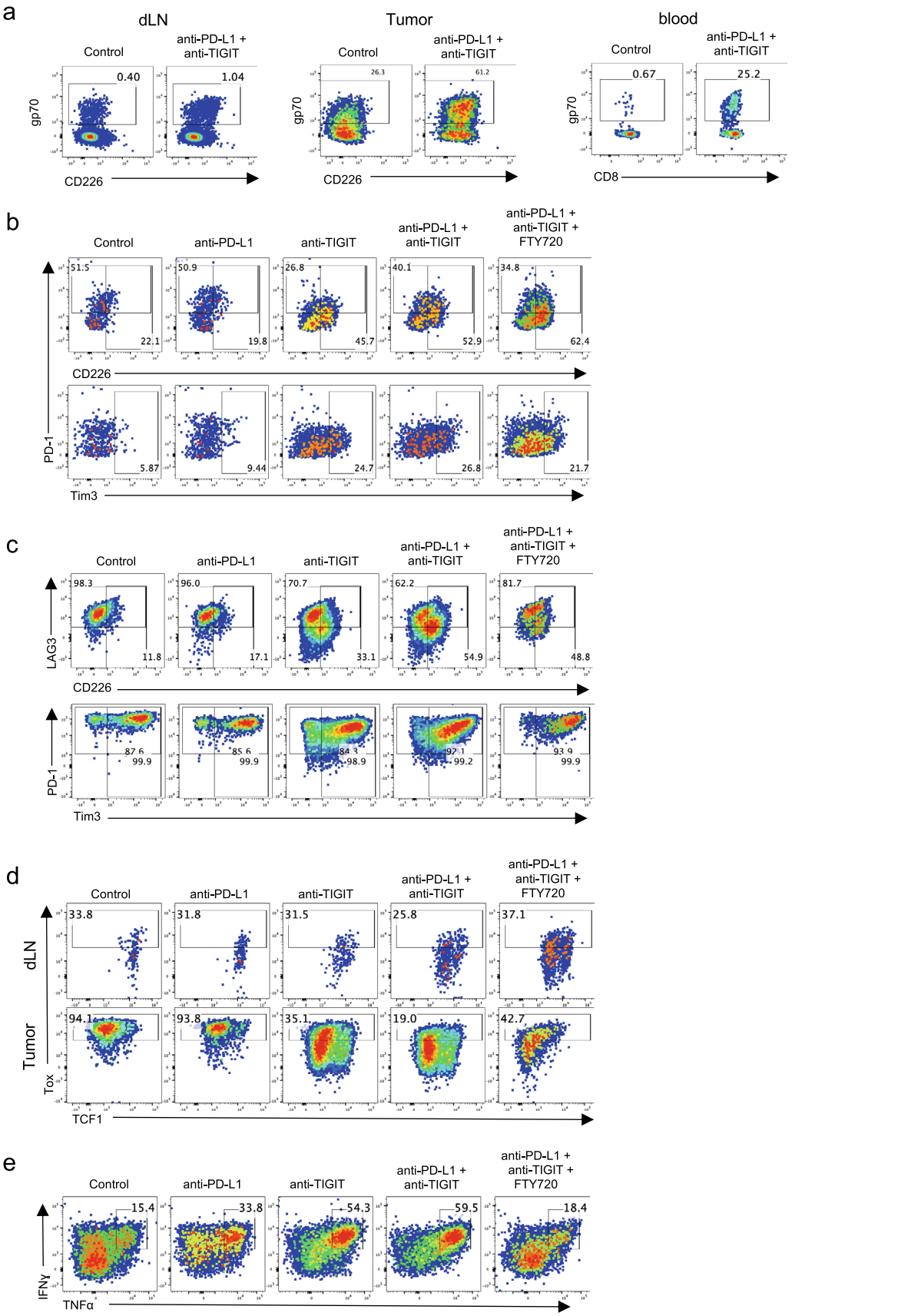

Extended Data Fig. 2 | Flow cytometry gating strategies. a, Representative dot plots for CD226 and gp70 tetramer co-expression on CD8$^+$ T cells in dLN or tumor, or gp70 tetramer staining on CD8$^+$ T cells in blood. **b**, Representative dot plots for CD226 and PD-1, Tim3 and PD-1 co-expression on CD8$^+$ T cells in dLN. **c**, Representative dot plots for CD226 and LAG3 or Tim3 and PD-1 co-expression on CD8$^+$ T cells in tumor. **d**, Representative dot plots for TCF1 and Tox co-expression on CD8$^+$ T cells in dLN or tumor. **e**, Representative dot plots for IFN-γ and TNF intracellular staining in CD8$^+$ T cells from tumor.

https://doi.org/10.1038/s43018-024-00870-6

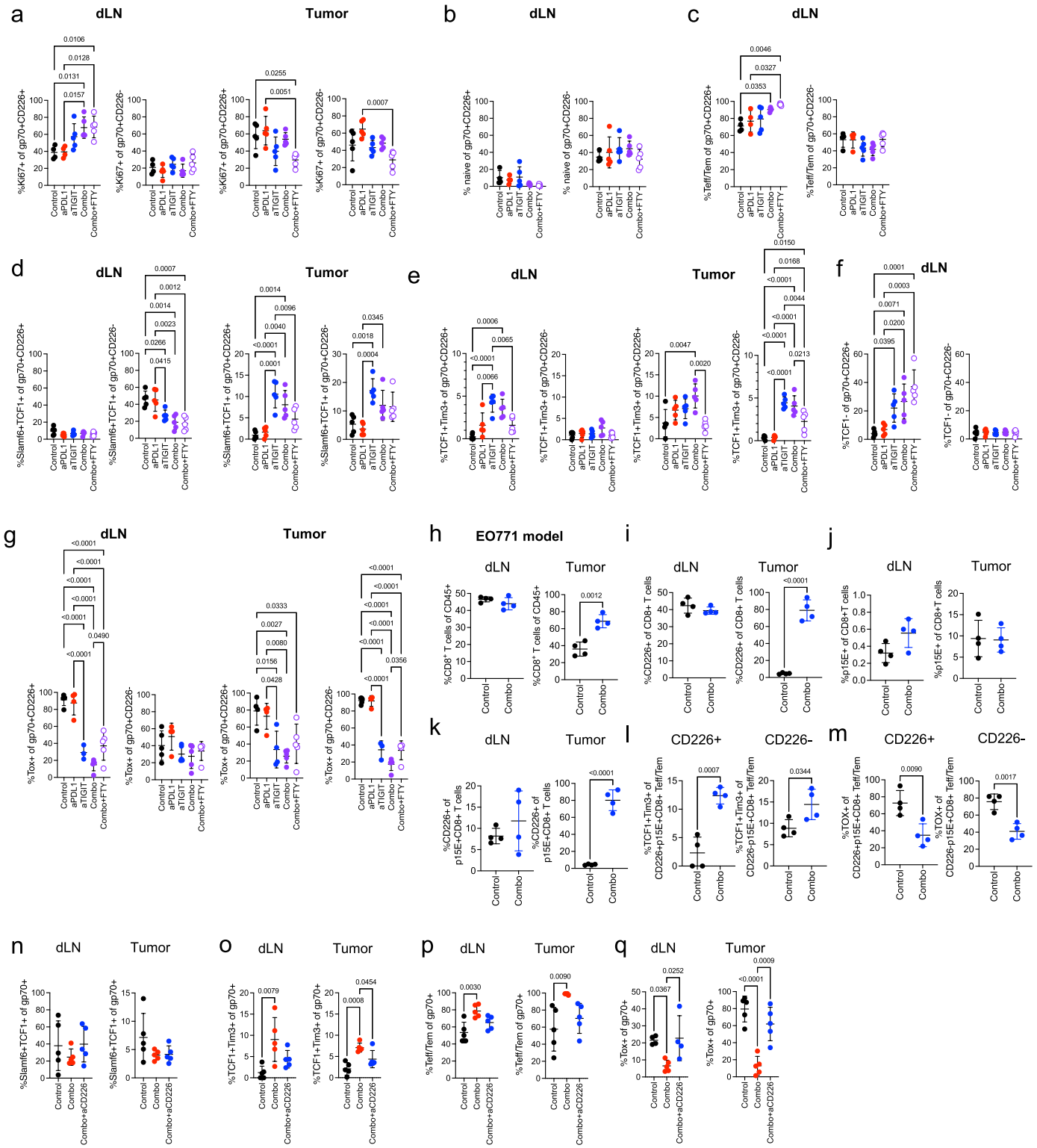

Extended Data Fig. 3 | See next page for caption.

https://doi.org/10.1038/s43018-024-00870-6

Extended Data Fig. 3 | Treatment effects on tumor-specific CD8$^+$ T cells. **a-g**, Phenotyping of CD226$^+$ or CD226$^-$ gp70$^+$ CD8$^+$ T cells from dLN or tumor, as indicated, of CT26 tumor-bearing mice treated with anti-PD-L1, anti-TIGIT, or combination with or without FTY720. Frequencies of gp70$^+$CD8$^+$ T cells expressing Ki67 (**a**), naïve phenotype (**b**), Teff/Tem phenotype (**c**), Slamf6 and TCF1 co-expression (**d**), TCF1 and Tim3 co-expression (**e**), not expressing TCF1 (**f**) or expressing Tox (**g**). For **a-g**, data are represented as mean +/- SD with individual symbols representing individual mice (n = 5 animals per sample and treatment group) and are representative of three independent experiments. *p*-values are indicated where differences between two groups were determined to be statistically significant by ordinary one-way ANOVA with Tukey's multiple comparisons test. **h-m**, anti-TIGIT plus anti-PD-L1 combination treatment increases frequencies of TCF1$^+$Tim$^+$ CD8$^+$ T cells and decreases frequencies of Tox$^+$ CD8$^+$ T cells in EO771 tumor-bearing mice. Mice with established EO771 tumors were treated with isotype control Ab or anti-TIGIT combined with anti-PD-L1, then dLN and tumors were collected on day 7 post-treatment for phenotypic characterization of CD8$^+$ T cells by flow cytometry. **h**, Frequencies of CD8$^+$ T cells in dLN (left) or tumor (right) as percentage of CD45$^+$ cells. **i**, Frequencies of CD8$^+$ T cells expressing CD226. **j**, Frequencies of CD8$^+$ T cells positively stained with tetramer against EO771-specific antigen p15E. **k**, Frequencies of p15E$^+$CD8$^+$ T cells expressing CD226. **l**, **m**, Frequencies of CD226$^+$ (left) or CD226$^-$ (right) p15E$^+$CD8$^+$ Teff/Tem cells co-expressing TCF1 and Tim3 (**l**) or Tox (**m**). For **h-m**, data are represented as mean +/- SD with individual symbols represent individual mice (n = 4 animals per sample and group); data are representative of one of two independent experiments. *p*-values are indicated where difference were determined by unpaired t-test to be statistically significant. **n-q**, Frequencies of gp70$^+$CD8$^+$ T cells co-expressing Slamf6 and TCF1 (**n**), co-expressing TCF1 and Tim3 (**o**), Teff/Tem phenotype (**p**) or Tox (**q**) in dLN (left) or tumor (right) of CT26 tumor-bearing mice treated with anti-PD-L1 plus anti-TIGIT combination or combo with anti-CD226 Ab. For **n-q**, data are represented as mean +/- SD with individual symbols representing individual mice (n = 5 animals per sample and treatment group) and are representative of three independent experiments. *p*-values are indicated where differences between two groups were determined to be statistically significant by ordinary one-way ANOVA with Tukey's multiple comparisons test.

https://doi.org/10.1038/s43018-024-00870-6

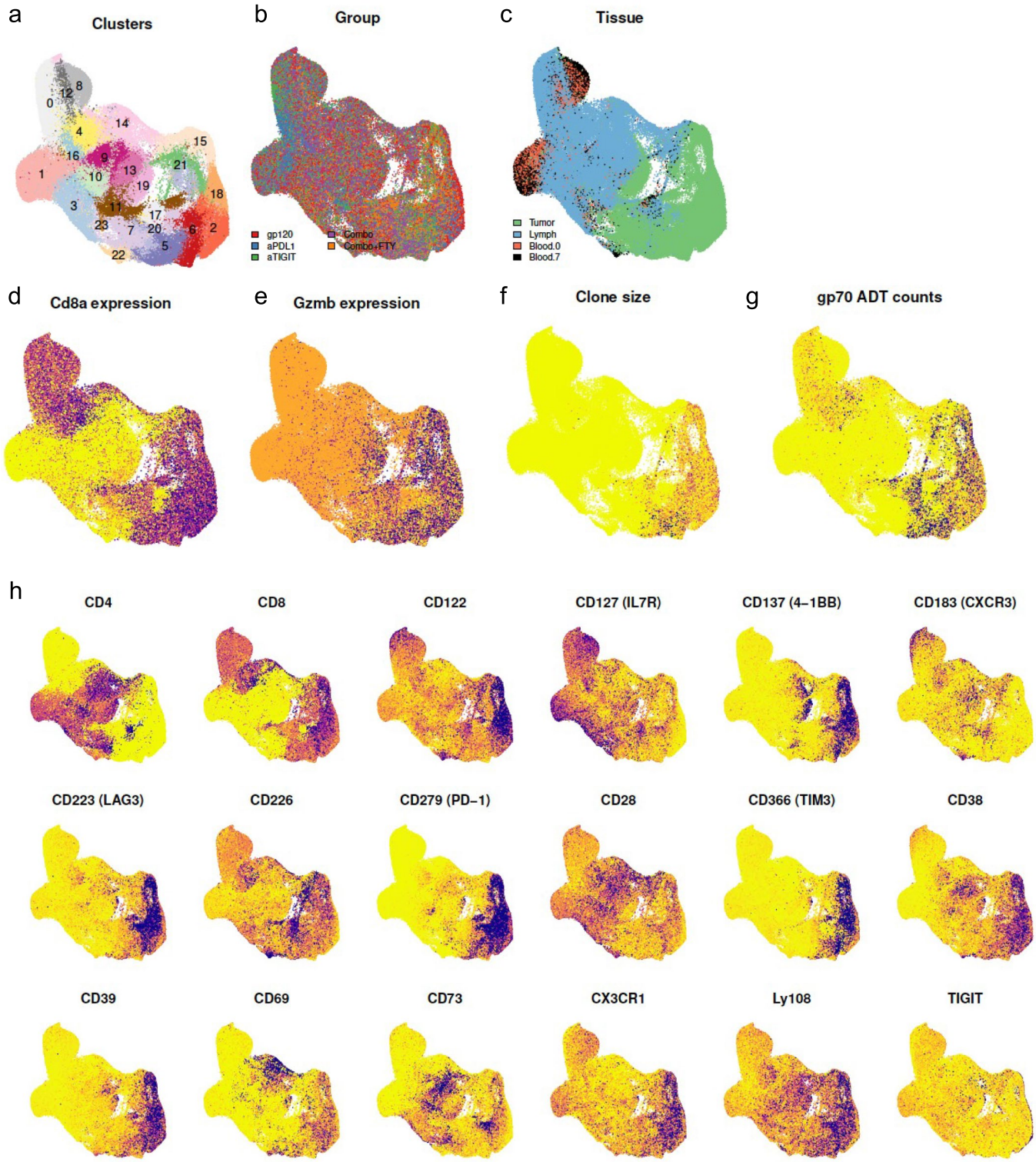

Extended Data Fig. 4 | Single-cell RNA-seq, TCR-seq and CITE-seq on 245,675 total T cells pooled from CT26 tumor, dLN and blood from 31 mice. a, UMAP showing T cell clusters representing $CD8^+$ T cells, $CD4^+$ T cells and regulatory T cells. **b,c**. Treatment group (Group) (**b**) or tissue source (**c**) of T cells. **d-g**. CD8a expression (**d**), granzyme B expression (**e**), clone size (**f**), gp70 ADT counts (**g**) projected on UMAP. **h**, CITE-seq relative expression levels for indicated markers are projected on UMAP.

https://doi.org/10.1038/s43018-024-00870-6

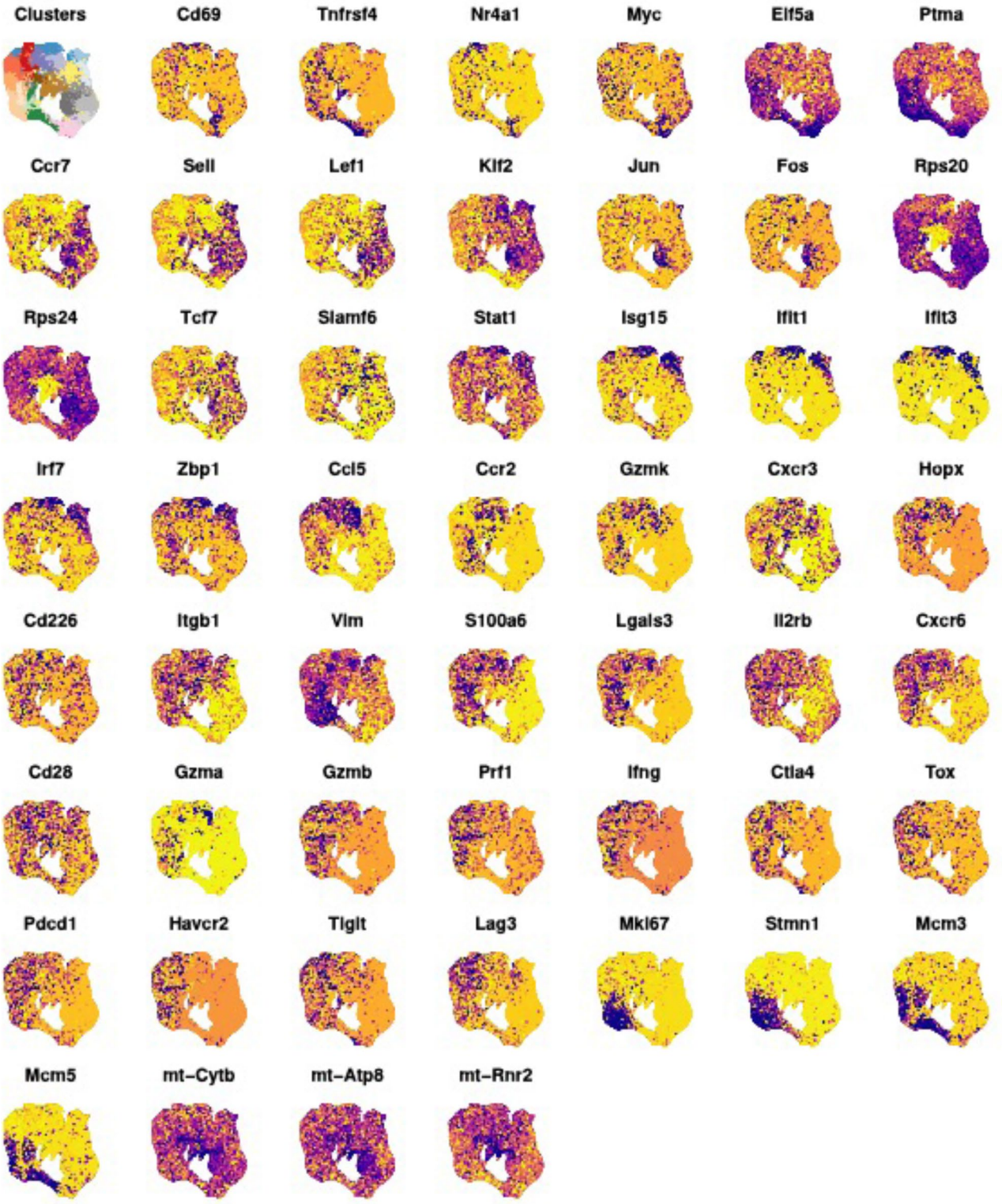

Extended Data Fig. 5 | CD8$^+$ T cell marker expression. Marker expression was measured by scRNA-seq and projected on UMAPs comprised of CD8$^+$ T cells from CT26 tumor, dLN and blood. n = 155,496 cells in all plots.

https://doi.org/10.1038/s43018-024-00870-6

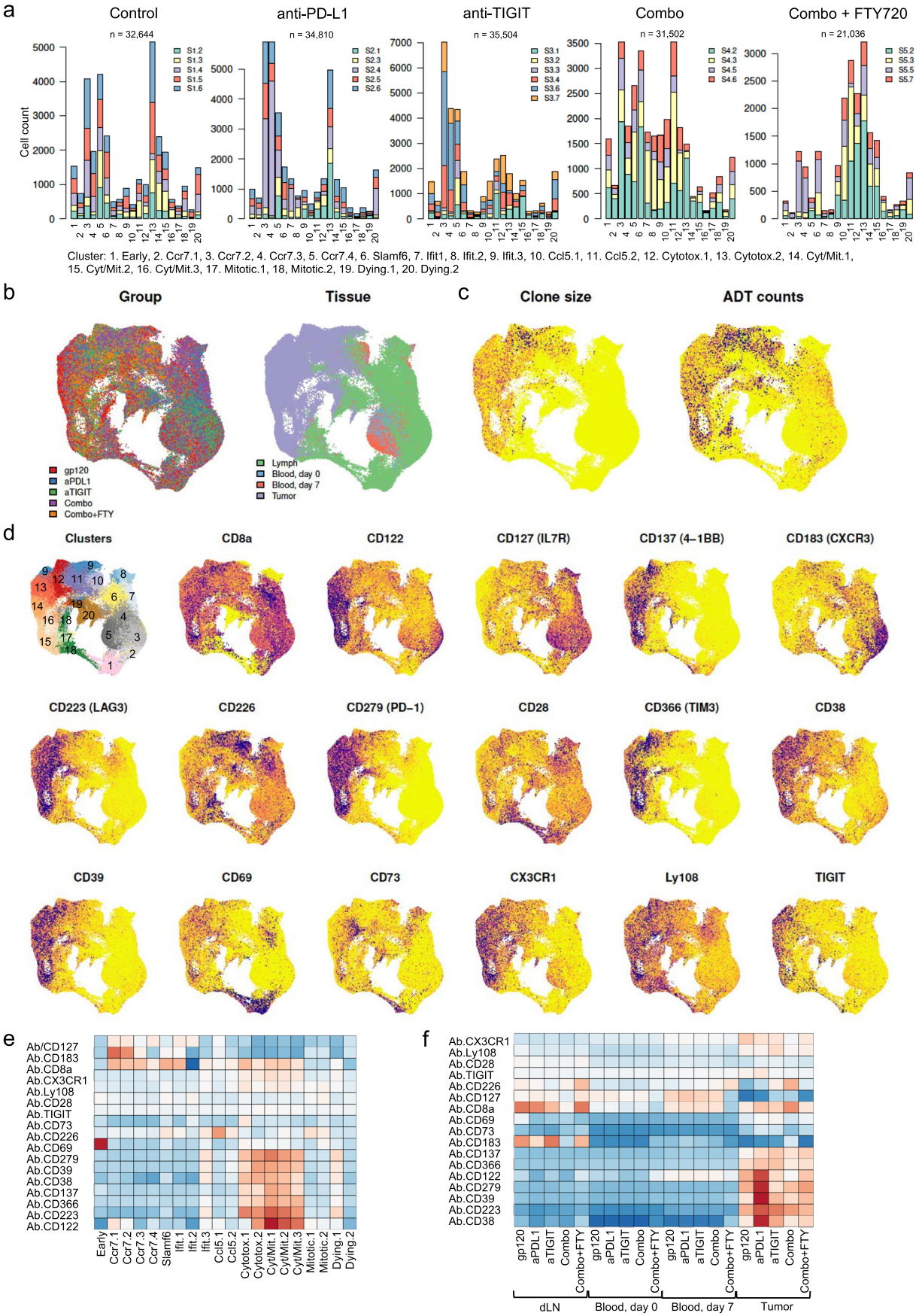

Extended Data Fig. 6 | See next page for caption.

https://doi.org/10.1038/s43018-024-00870-6

Extended Data Fig. 6 | Multiomic analysis of CD8$^+$ T cells. a, CD8$^+$ T cell cluster composition by individual mice in each treatment group. Each color represents an individual mouse. Data show that no cluster came solely from a single animal or experimental group. **b**, Treatment group (Group) and tissue source projected on CD8$^+$ T cell UMAP. **c**, Clone size and ADT counts projected on CD8$^+$ T cell UMAP. In panels (**b**) and (**c**), n = 155,496 cells. **d**–**f**. CD8$^+$ T cell marker expression measured by CITE-seq. **d**, Relative marker expression levels determined using CITE-seq antibodies projected on UMAPs comprised of CD8$^+$ T cells from CT26 tumor, dLN and blood. **e**, Heatmap of relative CITE-seq marker expression levels in each CD8$^+$ T cell cluster. **f**, Heatmap of relative CITE-seq marker expression levels in tissues under various treatment conditions.

https://doi.org/10.1038/s43018-024-00870-6

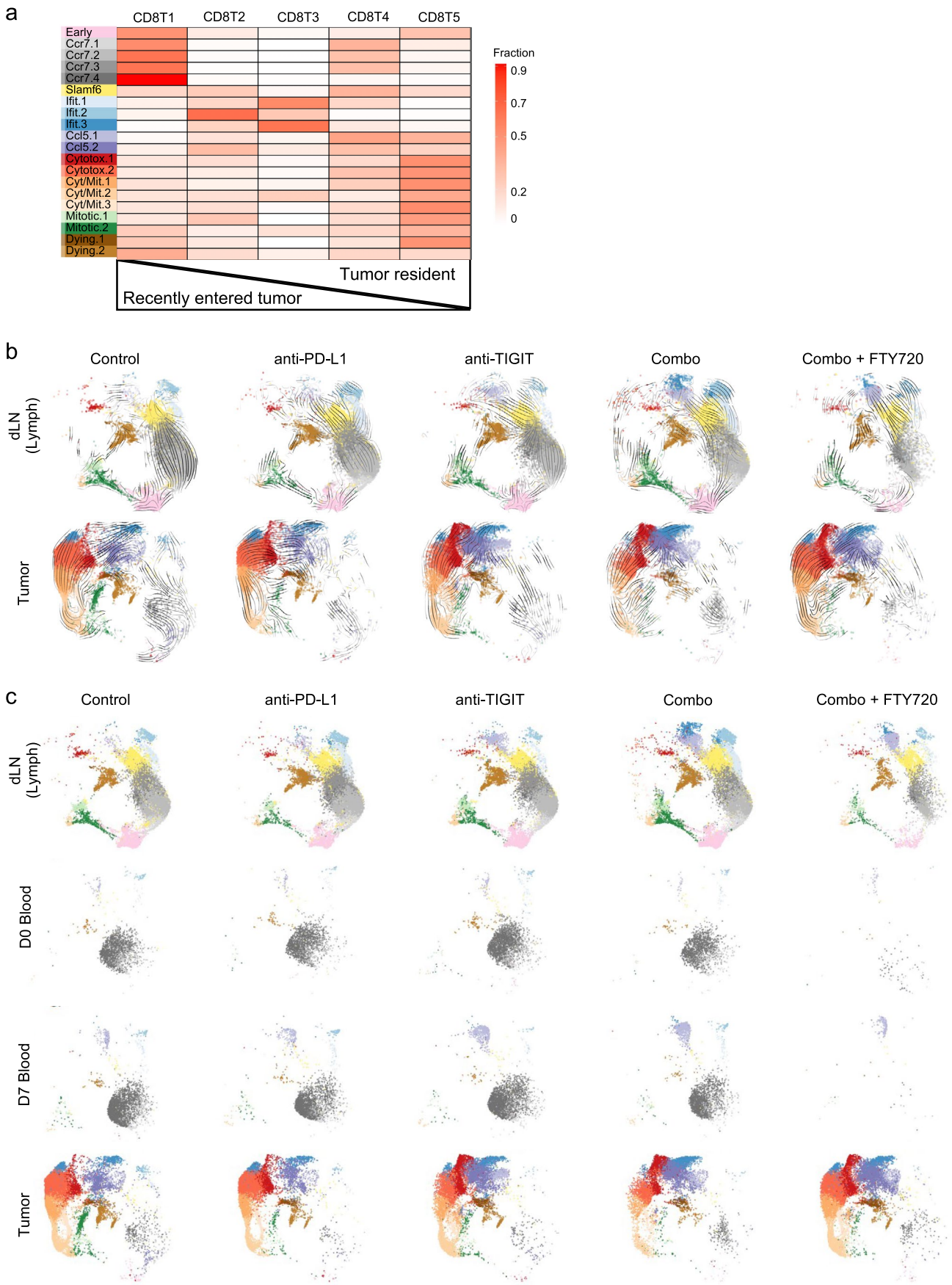

Extended Data Fig. 7 | See next page for caption.

https://doi.org/10.1038/s43018-024-00870-6

Extended Data Fig. 7 | Characterization of CD8$^+$ T cell clusters. a, Heatmap showing clusters defined using metadata from Li et al.[24], where CD8T1 are likely naïve, CD8T2 has Tscm/memory properties, CD8T4 has activated effector cell properties, and CD8T5 has an exhausted phenotype. CD8T1 and CD8T2 were described as T cells that recently entered the tumor, while CD8T4 and CD8T5 were cells resident in tumor. CD8T2 also have the capacity to recirculate from tumor to dLN. **b**, RNA velocity projections on UMAPs for each treatment group in dLN (top) and tumour (bottom). **c**, UMAPs showing cluster composition in dLN (Lymph), tumor and blood from CT26 tumor-bearing mice treated with isotype control, anti-PD-L1, anti-TIGIT, combination, or combination with FTY720.

https://doi.org/10.1038/s43018-024-00870-6

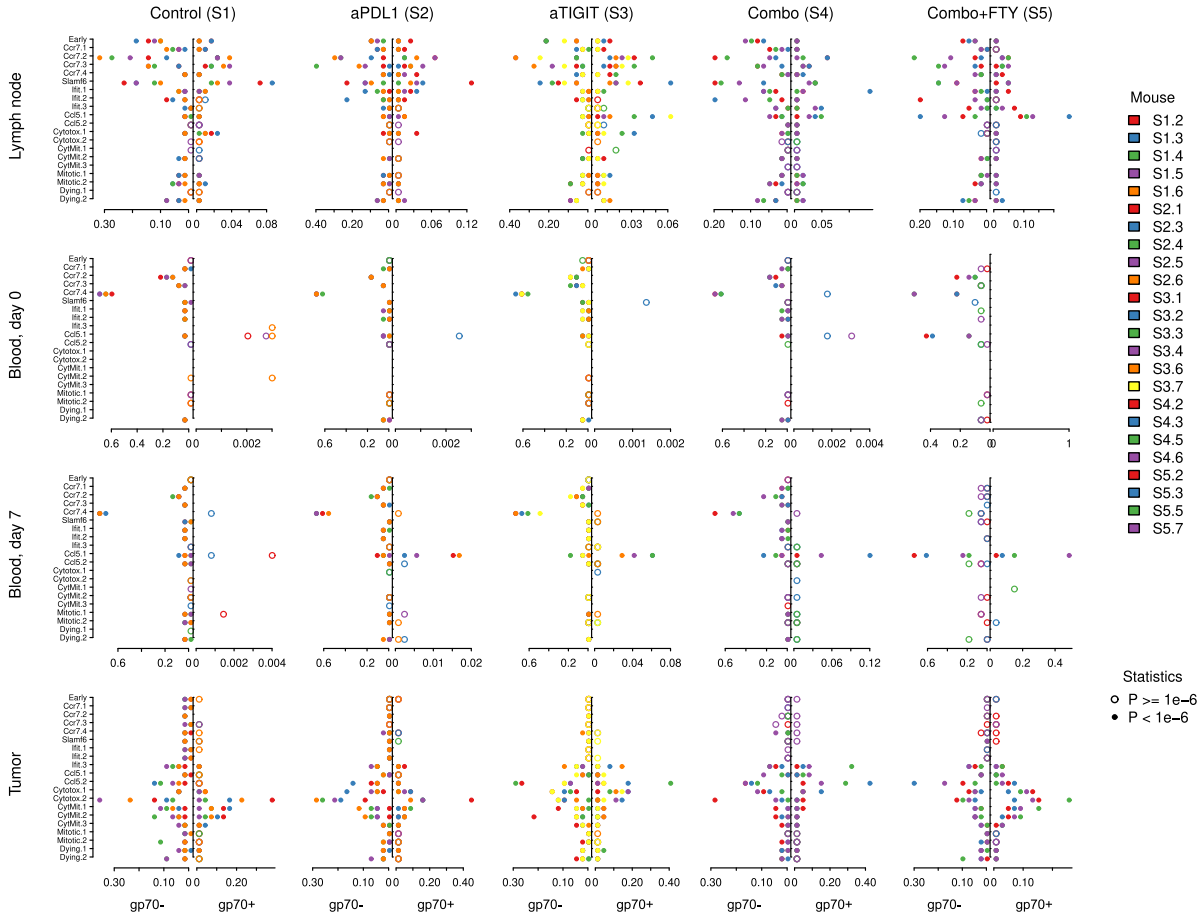

Extended Data Fig. 8 | Characterization of tumor-specific CD8⁺ T cell cluster composition. CD8⁺ T cell cluster composition segregated by specificity for gp70, determined by comparing ADT counts for gp70 tetramers, requiring that they be higher than control tetramer count by a Poisson test with a one-sided p-value < 1×10^{-6}. The proportion of each cluster within total CD8⁺ T cells from the indicated tissue for each treatment group is shown. Each symbol represents an individual mouse; each color identifies the same mouse within the treatment group.

https://doi.org/10.1038/s43018-024-00870-6

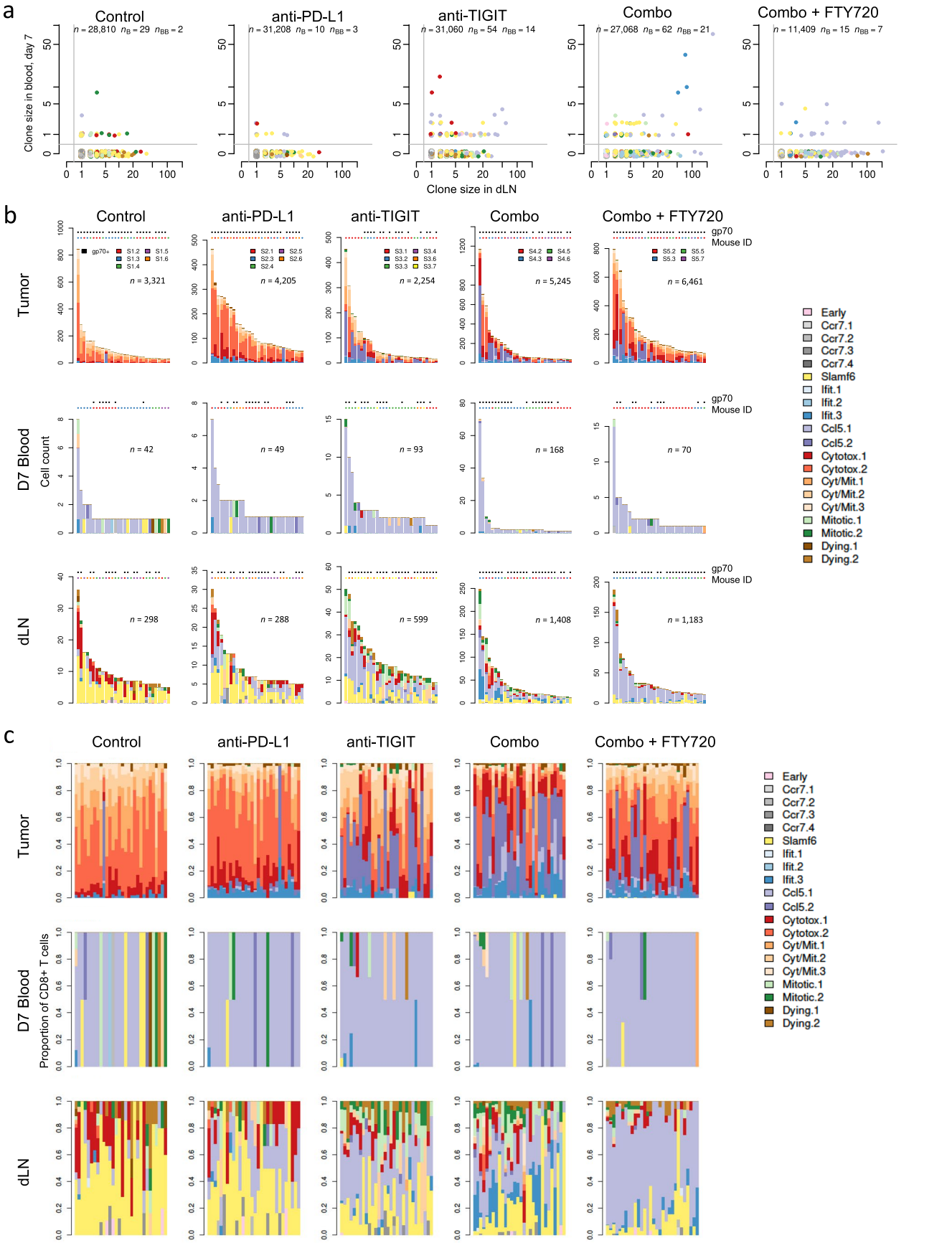

Extended Data Fig. 9 | See next page for caption.

https://doi.org/10.1038/s43018-024-00870-6

Extended Data Fig. 9 | Clonal diversity of CD8$^+$ T cells. a, Scatterplots showing primary clusters of each individual clonotype in dLN and blood at day 7 (D7 Blood). *n* represents the total number of clones within a cluster in each scatterplot; n_B is the number of clones observed in blood at day 7; n_{BB} is the number of clones in blood at day 7 with clone size greater than 1. Color of circles denote cluster designation as shown in panels (**b**) and (**c**). **b, c**, Cluster composition for the 30 largest clonotypes from tumor (upper panels), D7 blood (middle panels) or dLN (lower panels) of CT26 tumor-bearing mice treated with isotype control, anti-PD-L1, anti-TIGIT, combination, or combination with FTY720, shown as (**b**) absolute numbers, or (**c**) normalized against the total number of cells for each individual clonotype (total cell number = 1). Cluster identity is indicated by color. In (**b**), clonotypes from individual mice within each treatment group are identified by the color legend at the top of the tumor bar graphs. Individual mice are labeled as S"group number"."mouse number". gp70$^+$ clones are identified by black symbol at the top of the bar graphs.

https://doi.org/10.1038/s43018-024-00870-6

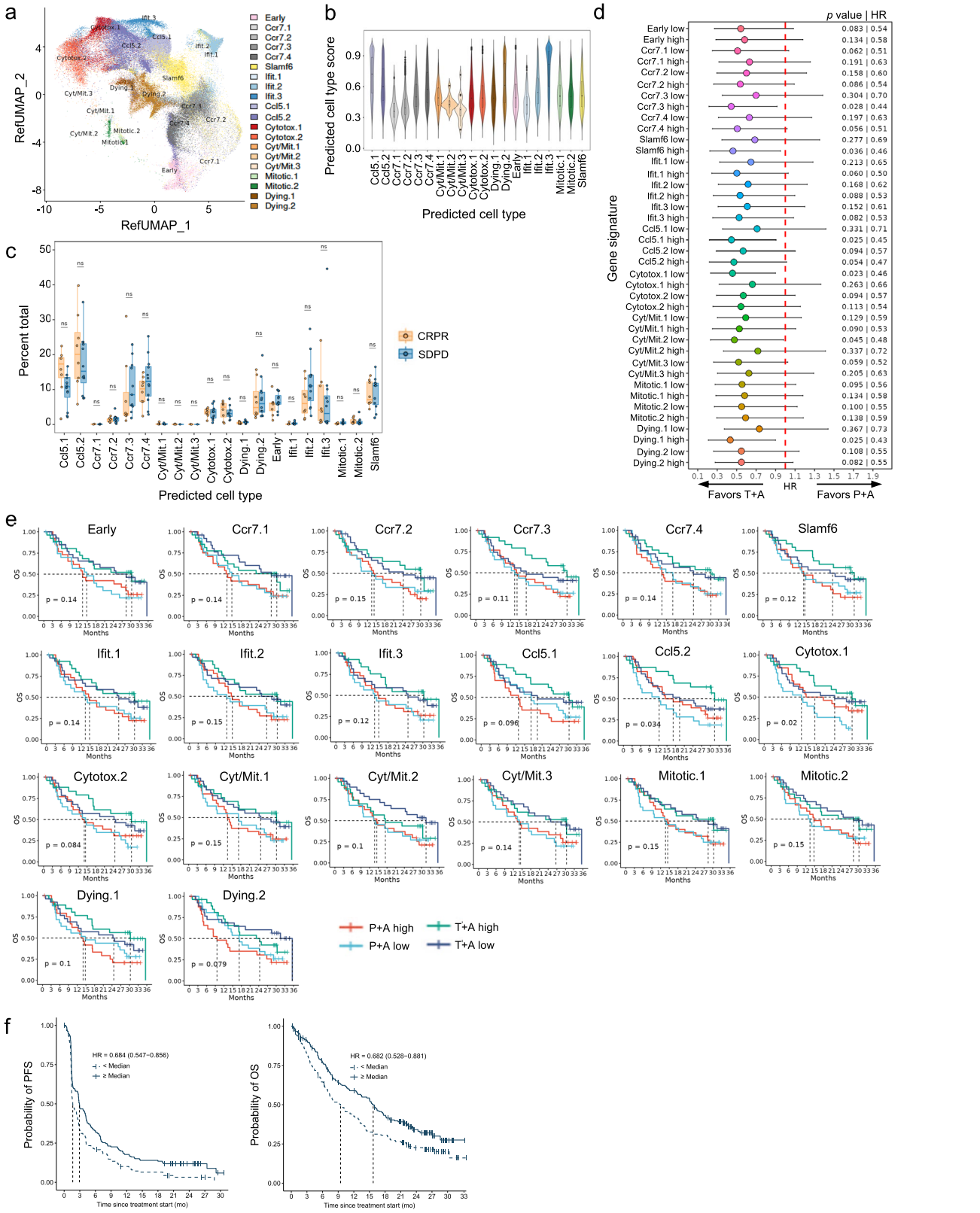

Extended Data Fig. 10 | See next page for caption.

https://doi.org/10.1038/s43018-024-00870-6

Extended Data Fig. 10 | Analysis of human CD8$^+$ T cell clusters. Association of human CD8$^+$ T cell clusters corresponding to mouse reference with response in tiragolumab plus atezolizumab Ph1b and Ph2 NSCLC clinical trials. **a**. scRNA-seq of 144,413 human CD8$^+$ T cells from blood of patients in a Ph1b NSCLC study of tiragolumab plus atezolizumab (T + A). Human genes were renamed to their mouse ortholog (if present) and gene expression was normalized before sample integration and projection onto a mouse CD8$^+$ T cell reference UMAP. **b**. Predicted cell type score for mapped human CD8$^+$ T cells for each assigned mouse CD8$^+$ T cell reference cluster. **c**. Frequencies of human predicted clusters in patients with complete or partial response (CRPR) compared to stable or progressive disease (SDPD) on cycle 2 day 1 of treatment with T + A in the Ph1b study. Percent total was calculated as the percentage of the cluster in total CD8$^+$ T cells for each patient. **d**. Forest plot comparing high or low expression of the top corresponding human 18-20 signature genes (signature gene score) from each mouse CD8$^+$ T cell cluster or *CD8A* and their association with overall survival (OS) hazard ratio (HR) T + A or placebo plus atezolizumab (P + A) treatment groups in Ph2 CITYSCAPE. Mean HR with 95% confidence intervals and *p*-values are shown. **e**, Kaplan-Meier curves showing OS probability in P + A or T + A treatment groups dichotomized on the basis of high or low CD8$^+$ T cell cluster gene scores from each reference cluster. *p*-value is from log-rank test with null hypothesis that there is no difference between the groups. **f**. Kaplan-Meier curves comparing progression-free survival (PFS, left) or OS (right) in patients from the phase 3 NSCLC OAK study who received atezolizumab monotherapy. Patients were dichotomized by median gene score calculated using the average expression of the CD8 gene panel comprised of *CXCR3*, *CXCR6* and *CCL5*.

nature portfolio

Corresponding author(s): Eugene Chiang and Ira Mellman

Last updated by author(s): Oct 9, 2024

Reporting Summary

Nature Portfolio wishes to improve the reproducibility of the work that we publish. This form provides structure for consistency and transparency in reporting. For further information on Nature Portfolio policies, see our Editorial Policies and the Editorial Policy Checklist.

Statistics

For all statistical analyses, confirm that the following items are present in the figure legend, table legend, main text, or Methods section.

n/a	Confirmed
☐	☒ The exact sample size (*n*) for each experimental group/condition, given as a discrete number and unit of measurement
☐	☒ A statement on whether measurements were taken from distinct samples or whether the same sample was measured repeatedly
☐	☒ The statistical test(s) used AND whether they are one- or two-sided *Only common tests should be described solely by name; describe more complex techniques in the Methods section.*
☒	☐ A description of all covariates tested
☐	☒ A description of any assumptions or corrections, such as tests of normality and adjustment for multiple comparisons
☐	☒ A full description of the statistical parameters including central tendency (e.g. means) or other basic estimates (e.g. regression coefficient) AND variation (e.g. standard deviation) or associated estimates of uncertainty (e.g. confidence intervals)
☐	☒ For null hypothesis testing, the test statistic (e.g. *F*, *t*, *r*) with confidence intervals, effect sizes, degrees of freedom and *P* value noted *Give P values as exact values whenever suitable.*
☒	☐ For Bayesian analysis, information on the choice of priors and Markov chain Monte Carlo settings
☒	☐ For hierarchical and complex designs, identification of the appropriate level for tests and full reporting of outcomes
☒	☐ Estimates of effect sizes (e.g. Cohen's *d*, Pearson's *r*), indicating how they were calculated

Our web collection on statistics for biologists contains articles on many of the points above.

Software and code

Policy information about availability of computer code

Data collection

FACS data was acquired on LSR-Fortessa or BD Symphony instruments using FACSDiva version 8.0.1 or Cytek Aurora using SpectroFlo version v3.0.3. Processing for single-cell gene expression (scRNA-seq) and T cell receptor V(D)J clonotypes (scTCR-seq) was done using the Chromium Single Cell 5' Library and Gel Bead Kit (10X Genomics), following manufacturer's instructions. Sequencing files from Illumina assays were run through CellRanger version 6.1.1 against a transcriptome derived from ENSEMBL version 2.2.0 for the mouse genome GRCm38. The combined matrix files from the filtered_feature_bc_matrix directory for the RNA and ADT libraries were divided into separate submatrices for each sample, based on 52,636 genes for expression, 6 tetramer barcodes for ADT counts, 24 antibody measurements for CITE-seq, and 10 barcodes for multiplexing of the blood samplees. Measurements corresponding to various alleles of T cell receptor genes (e.g., Trbv1 through Trbv31) were combined into a single gene measurement (Trbv). Single cells from pooled blood samples were demultiplexed as described in the Methods section.

Data analysis

FACS analysis was performed using FlowJo version 10 or higher, and figures were generated using GraphPad Prism version 9.4.1. Mouse single-cell analyses were performed in R version 4.2.0 and with scripts written for Perl version 5.16.3. Single-cell UMI count matrix for each tissue sample was processed using scDblFinder version 1.12.0. Remaining singlet count matrices were processed using Seurat version 4.1.1. using the SCTransform function. Additional analysis was performed using Seurat procedures NormalizedData, FindVariableFeatures, ScaleData,RunPCA, RunUMAP, FindNeighbors, FindClusters. Batch correction was performed using Harmony package 0.1.1. PCA cell embeddings were calculated following the procedure in https://cran.r-project.org/web/packages/harmony/vignettes/Seurat.html. Additional analysis was performed using Matrix 1.4-1, sparseMatrixStats version 1.8.0, SingleR version 1.10.0, superheat version 1.0.0, and RColorBrewer version 1.1-3. RNA velocity analysis was performed using kallisto bustools (version 0.46.1), with mapping to a transcriptome index from Ensembl version 90 on genome GRCm38. The transcriptome index was generated using kallisto with a read length of 90 nucleotides and intronic sequences from BUSpaRse (https://github.com/BUStools/BUSpaRse). Objects were processed by scvelo package 0.2.4 within Python version 3.7.3 using the commands "pp.filter_and_normalize", "pp.moments", "Tl.recover_dynamics" and "Tl.velocity" with mode="dynamical."

Velocity graphs were generated using the command "tl.velocity_graph" and "pl.velocity_embedding_stream."Additional figures were generated using Adobe Illustrator (version 27.0 or higher) and BioRender. External datasets were obtained from NCBI GEO and ArrayExpress, with metadata provided directly from authors by direct request or cell assignments from the Seurat object provided online, as described in the Methods section. Analysis of clinical trial data was performed using R version 4.2.0. Human genes were converted to their mouse orthologs using babelgene version 22.9. Human CD8+ T cells were then separated by patient and normalized with SCTransform in Seurat version 4.2 using default parameters. MapQuery function in Seurat was used to transfer cell type labels, integrate embeddings and to project the query data onto the reference UMAP. , R version 4.2.0 packages survminer version 0.4.9 and survival 3.4-0 were used to generate Kaplan-Meier plots. Computer code used to generate the single-cell analyses and figures in this paper are provided as a Supplementary File to the NCBI GEO accession GSE220901.

Computer code used to generate the single-cell analyses and figures in this paper are provided as a Supplementary File to the NCBI GEO accession GSE220901. Code for reanalyzed datasets from GO30103 (NCT02794571) (Ref 4,31), CITYSCAPE (NCT03563716) (Ref 3,4), and OAK (NCT02008227) (Ref 4,32) clinical trials are accessible at https://github.com/cwtran/nutsch_nature_cancer_2024/.

For manuscripts utilizing custom algorithms or software that are central to the research but not yet described in published literature, software must be made available to editors and reviewers. We strongly encourage code deposition in a community repository (e.g. GitHub). See the Nature Portfolio guidelines for submitting code & software for further information.

Data

Policy information about availability of data

All manuscripts must include a data availability statement. This statement should provide the following information, where applicable:

- Accession codes, unique identifiers, or web links for publicly available datasets
- A description of any restrictions on data availability
- For clinical datasets or third party data, please ensure that the statement adheres to our policy

FASTQ files containing raw sequencing reads for the scRNA-seq, scTCR-seq, ADT-seq, and CITE-seq analyses have been deposited with the NCBI Short Read Archive (SRA) under accession PRJNA911822. Processed output files from Cell Ranger and metadata with cluster assignments, clonotypes, and ADT assignments have been deposited with the NCBI Gene Expression Omnibus (GEO) under accession GSE220901. Raw counts and metadata for reanalyzed scRNAseq data from GO30103 (NCT02794571) (Refs (4,31) are available from the European Genome-Phenome Archive (EGA) under accession EGAD50000000367 and https://github.com/cwtran/nutsch_nature_cancer_2024/. Reanalyzed datasets from CITYSCAPE (NCT03563716) (Refs 3,4) and OAK (NCT02008227) (Refs 4,32) clinical trials can be found under EGA accession EGAD50000000251 and EGAD50000000368, respectively. All data relating to mouse sequencing data at NCBI SRA and NCBI GEO and pseudoanonymized clinical trial data are available without restrictions. Due to legal requirements for data sharing, users must agree to the Data Access Agreement detailed in the EGA entries above before they can access these human datasets. Data access requests are reviewed by the Genentech DevSci Data Access Committee (devsci-dac-d@gene.com).

Reanalysis of previously published datasets generated by others and publicly available was as follows: for Huang et al., 2022 (Ref 16), we used metadata provided by the authors to us and scRNA-seq count data for the six samples referenced in the metadata from NCBI GEO for GSE180095, GSE122712, GSE152628, and GSE182509; for Daniel et al., 2022 (Ref 24), we used metadata from supplementary files and the scRNA-seq count data, both available at NCBI GEO for GSE188666; for Deak et al., 2022 (Ref 25), we used metadata provided by the authors to us, and scRNA-seq count data available at ArrayExpress for E-MTAB-11773; for Giles et al., 2022 (Ref 26), we used metadata from the Seurat object through the link provided in their paper under Data Availability and scRNA-seq count data available at NCBI GEO for GSE199563; for Li et al., 2022 (Ref 28), we used metadata (taking cluster assignments for celltype_cluster-2) and scRNA-seq normalized data from the Scanpy object available at ArrayExpress for E-MTAB-10176.

Source data for Fig. 1, 2a, 2d, 2e, 3b, 3c, 4, 5c, 6a, 6b, 6c and Extended Data Fig. 1b, 1c, 3a-q, 6a, 6e, 7a, 8, 9b, 9c have been provided as Source Data files. All other data supporting the findings of this study are available from the corresponding author on reasonable request.

Research involving human participants, their data, or biological material

Policy information about studies with human participants or human data. See also policy information about sex, gender (identity/presentation), and sexual orientation and race, ethnicity and racism.

Reporting on sex and gender	Sex and gender for subjects for the CITYSCAPE phase 2 clinical trial are described in the publication Cho et al., Tiragolumab plus atezolizumab versus placebo plus atezolizumab as a first-line treatment for PD-L1-selected non-small-cell lung cancer (CITYSCAPE): primary and follow-up analyses of a randomised, double-blind, phase 2 study, The Lancet 23, 781-792, 202 (Ref 3). The placebo plus atezolizumab group had a slightly higher proportion of male patients (48 [71%] versus 39 [58%]).
Reporting on race, ethnicity, or other socially relevant groupings	Population characteristics of subjects for the CITYSCAPE phase 2 clinical trial have been previously described (Ref 3).
Population characteristics	Population characteristics of subjects for the CITYSCAPE phase 2 clinical trial are also described in the publication above (Ref 3). Patients, irrespective of treatment arm, were separated on the basis of clinical response (complete response/partial response vs. stable disease/progressive disease). Baseline characteristics of the intention-to-treat (ITT) population include a median age of 68 years in both the tiragolumab + atezolizumab (T+A) or placebo + atezolizumab (P+A) treatment groups. The distribution by sex was 58% male to 42% female in the T+A arm and 71% male to 29% female in the P+A arm. ECOG status was 0 for approximately 30% of patients and 1 for 70% of patients for both treatment arms. 81% of NSCLC patients were stage IV in the T+A arm and 72% stage IV in the P+A arm. PD-L1 positivity by 22C3 was 57% at the 1-49% cutoff and 43% at the PD-L1 ≥ 50% cutoff for both treatment arms. Tumor histology was approximately 60% non-squamous and 40% squamous for both treatment arms. Approximately 10% of patients were never smokers, 65% previous smokers, and 25% current smokers for both arms. Patients with EGFR or ALK mutations were excluded from study.

Recruitment	Patients were recruited between Aug 10, 2018, and March 20, 2019. Of 275 patients assessed, 135 eligible patients were included in the study and randomly assigned to tiragolumab plus atezolizumab (n=67) or placebo plus atezolizumab (n=68), from across Europe (42%, n-57), Asia (31%, n=42) and the USA (27%, n=36).
Ethics oversight	Study design, patient cohort and response assessment for clinical trials GO30103 (NCT02794571) (Ref 31) and CITYSCAPE (NCT03563716) (Ref 3) have been previously described, with trial protocols approved by the institutional review board or ethics committee at each participating center and complied with good clinical practice guidelines, and studies performed in accordance with the principles of the Declaration of Helsinki, the International Council for Harmonization guidelines for Good Clinical Practice, and country-specific laws and regulations, as noted in the originally published clinical trials (Ref 3,31). GO30103 was conducted at 13 sites in 6 countries (Australia, Canada, France, South Korea, Spain, and the USA. CITYSCAPE was conducted in 41 clinical centers across France, Serbia, South Korea, Spain, Taiwan, and the USA. All patients provided written informed consent. An internal monitoring committee reviewed available safety data periodically to make recommendations regarding study conduct to ensure the safety of patients enrolled in the study, as noted in the originally published clinical trials (Ref 3,31).

Note that full information on the approval of the study protocol must also be provided in the manuscript.

Field-specific reporting

Please select the one below that is the best fit for your research. If you are not sure, read the appropriate sections before making your selection.

☒ Life sciences ☐ Behavioural & social sciences ☐ Ecological, evolutionary & environmental sciences

For a reference copy of the document with all sections, see nature.com/documents/nr-reporting-summary-flat.pdf

Life sciences study design

All studies must disclose on these points even when the disclosure is negative.

Sample size	No statistical methods were used to predetermine sample size. Sample sizes were based on previous experiences (Johnston, R. J. et al. The Immunoreceptor TIGIT Regulates Antitumor and Antiviral CD8+ T Cell Effector Function. Cancer Cell 26, 923-937, doi:10.1016/j.ccell.2014.10.018 (2014).), balancing animal welfare and statistical robustness.
Data exclusions	Animals whose tumors became ulcerated prior to progression or complete response or at time of allocation of experiment groups were euthanized and removed from the study. Single cells from blood and tumor were sorted by FACS to be CD90+. Single cells from draining lymph nodes were sorted to be CD90+CD44+. Single cells were further separated computationally to analyze CD8+ T cells in detail, as described in the Methods section.
Replication	The number of repeats and sample sizes are provided in each figure legend where applicable. All data were reliably reproducible.
Randomization	Tumor injected mice were randomly assigned to experimental groups. All UMAP figures plot cells in random order. Random jitter is added to scatterplots to visually display all points. For analysis of human clinical trial data, patients were separated on the basis of clinical responses, irrespective of treatment arm.
Blinding	Blinding was not relevant to this study and the data analysis of clinical trial biomarker data. Patients, irrespective of treatment arm, were separated on the basis of clinical response. The Phase 2 CITYSCAPE trial was a randomized, double-blind, placebo-controlled trial.

Reporting for specific materials, systems and methods

We require information from authors about some types of materials, experimental systems and methods used in many studies. Here, indicate whether each material, system or method listed is relevant to your study. If you are not sure if a list item applies to your research, read the appropriate section before selecting a response.

Materials & experimental systems

n/a	Involved in the study
☐	☒ Antibodies
☐	☒ Eukaryotic cell lines
☒	☐ Palaeontology and archaeology
☐	☒ Animals and other organisms
☐	☒ Clinical data
☒	☐ Dual use research of concern
☒	☐ Plants

Methods

n/a	Involved in the study
☒	☐ ChIP-seq
☐	☒ Flow cytometry
☒	☐ MRI-based neuroimaging

Antibodies

Antibodies used	All antibodies and dyes used for Flow analysis and/or FACS sorting for single cell analysis are provided as supplementary information.

Antibodies used

Fluorophore/Type; Target; Catalog Number; Supplier; Clone Number; Lot Number; Species
APC-Cy7 B220 103224 BioLegend RA3-6B2 B308558 Rat
PerCP-Cy5.5 B220 103235 BioLegend RA3-6B2 B308915 Rat
Dye Calcein blue C1429 Invitrogen n/a 2326042 n/a
APC-Cy7 CD11b 561039 BioLegend DX5 7278811 Rat
PerCP-Cy5.5 CD11b 101227 BioLegend M1/70 B308467 Rat
APC-Cy7 CD11c 117323 BioLegend N418 B197821 Armenian Hamster
PerCP-Cy5.5 CD226 133624 BioLegend TX42.1 B316769 Rat
BV785 CD226 133611 BioLegend TX42.1 B317733
BUV737 CD4 612843 BD Biosciences RM4-5 1198910 Rat
Qdot 605 CD4 50-113-7562 Invitrogen RM4-5 2366139 Rat
PE-Cy7 CD44 103030 BioLegend IM7 B308091 Rat
AF700 CD45 56-0441-82 Invitrogen IM7 1980496 Rat
BUV395 CD45 564279 BD Biosciences 30-F11 1145827 Rat
BV605 CD62L 104437 BioLegend MEL-14 B336181 Rat
BV421 CD69 104545 BioLegend H1.2F3 B291490 Armenian Hamster
AF700 CD8 100730 BioLegend 53-6.7 B285812 Rat
BUV737 CD8 564297 BD Biosciences 53.6-7 6294901 Rat
FITC CD8 100706 BioLegend 53.6-7 B318296 Rat
BV785 CD90.2 105331 BioLegend 30-H12 B289707 Rat
BUV395 CD90.2 565257 BD Biosciences 53-2.1 9311233 Rat
BUV805 CD90.2 741908 BD Biosciences 30-H12 2075373 Rat
eFluor 780 Fixable Viability Dye 65-0856-14 Invitrogen n/a 2450571 n/a
eFluor 506 FoxP3 69-5773-82 Invitrogen FJK-16s 2246975 Rat
pMHC Monomer gp70 n/a in house n/a n/a n/a
pMHC Monomor p15e n/a in house n/a n/a n/a
PE H3K27Me 40724S Cell Signaling C36B11 1 Rabbit
BV650 IFNy 563854 BD Biosciences XMG1.2 7096621 Rat
PE IL10 505008 BioLegend JES5-16E3 B249530 Rat
BV711 Ki67 350516 BioLegend Ki-67 B345424 Mouse
BUV737 Lag3 741820 BD Biosciences C9B7W 1333079 Rat
BV650 Lag3 125227 BioLegend C9B7W B309510 Rat
BUV496 Ly108/SlamF6 750046 BD Biosciences 13G3 2126118 Mouse
BV605 Ly108/SlamF6 745250 BD Biosciences 13G3 1068515 Mouse
PE-Cy7 PD-1 135216 BioLegend 29F.1A12 B355884 Rat
Dye Propidium Iodide 50-66211E Invitrogen n/a 9352710 n/a
BV650 Streptavidin 405231 BioLegend n/a B196153 n/a
PE TCF1/TCF7 14456S Cell Signaling C63D9 6147819 Rabbit
FITC TIGIT 11-9501-82 Invitrogen GIGD7 2318622 Rat
APC TIM3 134008 BioLegend B8.2C12 B198857 Rat
BV421 TIM3 134019 BioLegend B8.2C12 B321967 Rat
BV711 TIM3 119727 BioLegend RMT3-23 B284683 Rat
BV421 TNFa 506328 BioLegend MP6-XT22 B333754 Rat
APC Tox 130-118-474 Miltenyi Biotec REA473 5211104954 Human
Total-Seq C CD4 100571 BioLegend RM4-5 B318116
Total-Seq C CD8a 100785 BioLegend 53-6.7 B310956
Total-Seq C CD122 (IL-2Rβ) 105915 BioLegend 5H4 B315383
Total-Seq C CD127 (IL-7Rα) 135047 BioLegend A7R34 B300524
Total-Seq C CD137 (41BB) 106119 BioLegend 17B5 B305895
Total-Seq C CD183 (CXCR3) 126545 BioLegend CXCR3-173 B302524
Total-Seq C CD223 (LAG-3) 125237 BioLegend C9B7W B305125
Total-Seq C CD226 (DNAM-1) 128825 BioLegend 1.00E+06 B331517
Total-Seq C CD279 (PD-1) 109127 BioLegend RMP1-30 B300527
Total-Seq C CD28 102133 BioLegend 37.51 B304136
Total-Seq C CD366 (Tim-3) 119739 BioLegend RMT3-23 B302525
Total-Seq C CD38 102735 BioLegend 90 B299602
Total-Seq C CD39 143815 BioLegend DUHA59 B297080
Total-Seq C CD69 104551 BioLegend H1.2F3 B319428
Total-Seq C CD73 127237 BioLegend TY/11.8 B310991
Total-Seq C CX3CR1 149043 BioLegend SA011F11 B296692
Total-Seq C Ly108 134613 BioLegend 330-AJ B328193
Total-Seq C TIGIT (Vstm3) 142119 BioLegend IG9 B299596
Total-Seq C mouse IgG1 400187 BioLegend MOPC-21 B333559
Total-Seq C mouse IgG2 400293 BioLegend MOPC-173 B319350
Total-Seq C rat IgG1 400467 BioLegend RTK2071 B313972
Total-Seq C rat IgG2a 400577 BioLegend RTK2758 B307173
Total-Seq C rat IgG2b 400677 BioLegend RTK4530 B320446
Total-Seq C Arm Hamster 400977 BioLegend HTK888 B313973
Hashtags TotalSeq™-C0301 anti-mouse 155861 BioLegend M1/42; 30-F11 B325958
Hashtags TotalSeq™-C0302 anti-mouse 155863 BioLegend M1/42; 30-F12 B331515
Hashtags TotalSeq™-C0303 anti-mouse 155865 BioLegend M1/42; 30-F13 B332386
Hashtags TotalSeq™-C0304 anti-mouse 155867 BioLegend M1/42; 30-F14 B296942
Hashtags TotalSeq™-C0305 anti-mouse 155869 BioLegend M1/42; 30-F15 B339941
Hashtags TotalSeq™-C0306 anti-mouse 155871 BioLegend M1/42; 30-F16 B322559
Hashtags TotalSeq™-C0307 anti-mouse 155873 BioLegend M1/42; 30-F17 B323978
Hashtags TotalSeq™-C0308 anti-mouse 155875 BioLegend M1/42; 30-F18 B322555

Hashtags TotalSeq™-C0309 anti-mouse 155877 BioLegend M1/42; 30-F19 B328421
Hashtags TotalSeq™-C0310 anti-mouse 155879 BioLegend M1/42; 30-F20 B322104

Antibodies used for in vivo injection
Target; Catalog Number; Supplier; Clone Number; Lot Number; Species, Amount
anti-PD-L1 n/a GNE-in house 6E11 n/a n/a 10 mg/kg
anti-TIGIT (IgG2a; LALAPG) n/a GNE-inhouse 10A7 n/a n/a 10mg/kg
anti-gp120 n/a GNE-in house 3E5 n/a n/a 10mg/kg

Validation

For Flow analysis and FACS sorting, all the commercial antibodies were validated by the manufactures and prior studies of others. BD Biosciences antibody validation was performed as described by the manufacturer: "The specificity is confirmed using multiple methodologies that may include a combination of flow cytometry, immunofluorescence, immunohistochemistry or western blot to test staining of a combination of primary cells, cell lines or transfectant models" (https://bdbiosciences.com/en-us/products/reagents/flow-cytometry-reagents/research-reagents/quality-and-reproducibility). For BioLegend flow cytometry reagents, validation was performed as described by the manufacturer: "Specificity testing of 1-3 target cell types with either single- or multi-color analysis (including positive and negative cell types)" (https://www.biolegend.com/en-us/quality/quality-control). Certificates of analysis for Biolegend lots are available at http://biolegend.com/en-us/quality/quality-assurance-certificates. Quality certificate for BD Biosciences lots are available at http://regdocs.bd.com/regdocs/searchCOAAction.do. Quality certificates for Invitrogen lots are available at https://www.thermofisher.com/search/results?docTypes=COA&persona=DocSupport&linkIn=true. Additionally, changes in biological patterns of cellular markers of interest were monitored by using FMO or an isotype control. Selected titration of murine antibodies were determined on spleens or TILs of tumor bearing mice.

In-vivo antibodies (anti-gp120, anti-TIGIT, anti-PD-L1) were validated from prior publications (Johnston, R. J. et al. The Immunoreceptor TIGIT Regulates Antitumor and Antiviral CD8+ T Cell Effector Function. Cancer Cell 26, 923-937, doi:10.1016/j.ccell.2014.10.018 (2014).)

Eukaryotic cell lines

Policy information about cell lines and Sex and Gender in Research

Cell line source(s)	CT26 (ATCC - CRL2638), EO771 (ATCC - CRL3461)
Authentication	CT26 or EO771 cells were purchased from ATCC with corresponding certificates of analysis
Mycoplasma contamination	Cells were maintained at a dedicated internal cell line facility and tested to be mycoplasma-free.
Commonly misidentified lines (See ICLAC register)	No commonly misidentified lines were used in this study

Animals and other research organisms

Policy information about studies involving animals; ARRIVE guidelines recommended for reporting animal research, and Sex and Gender in Research

Laboratory animals	BALB/c or C57BL/6 mice were purchased from the Charles River or Jackson Laboratories. Mice were housed under specific-pathogen-free conditions at the Genentech animal facility. Mice were maintained in accordance with the Guide for the Care and Use of Laboratory Animals (National Research Council, 2011). Genentech is an American Association of Laboratory Animal Care (AAALAC)-accredited facility and all animal activities in this research study were conducted under protocols approved by the Genentech Institutional Animal Care and Use Committee (IACUC). Mice were housed in individually ventilated cages within animal rooms maintained under a 14h–10h light–dark cycle. Animal rooms were temperature and humidity controlled between 68 and 79°F (20.0 to 26.1°C) and from 30% to 70%, respectively, with 10 to 15 room air exchanges per hour. Female mice (aged 6-8 weeks) that appeared healthy and free of obvious abnormalities were used for the study. The maximum tumor size approved by IACUC was 2,000 mm3. Animals bearing tumors exceeding 2,000 mm3 or showing ulceration were euthanized following protocols approved by IACUC. Tumors were measured 3 times per week. In the case of tumors exceeding 2,000 mm3, tumor measurement was recorded prior to euthanasia. To minimize the number of mice with tumors exceeding 2,000 mm3, mice were euthanized if tumors were measured at greater than 1,700 mm3 on any given day, as tumor growth rate would make it highly likely for the tumor to exceed 2,000 mm3 by the next measurement. However, despite these measures, some tumors grew in excess of 2.000 mm3 between two measurements, as outlined here. In Fig. 1a, 8 mice were euthanized with tumors >1,700 mm3, 8 mice with tumors >2,000 mm3, 44 mice with ulcerations, and 1 mouse for other reason, across the entire study. In Fig. 1c, 5 mice were euthanized with tumors >2,000 mm3, 11 mice before tumors reached 2,000 mm3, and 1 mouse with ulceration, across the entire study. Details for experimental groups and individual mice are provided in Fig. 1 Source Data. In Extended Data Fig. 1b, 34 mice were euthanized with tumors >1,700 mm3, 26 mice with tumors >2,000 mm3, and 8 mice with ulcerations, across the entire study. Details for experimental groups and individual mice are provided in Extended Data Fig. 1 Source Data.
Wild animals	No wild animals were used.
Reporting on sex	C57BL/6 female mice were used wtih EO771 tumor studies as this line is derived and isolated from the mammary gland of a mouse with breast carcinoma. This study used genetically identical female mice to minimize biological variability, especially since androgen has been shown to affect gene expression in T cells.
Field-collected samples	No samples were collected from the field.

Ethics oversight	All experimental animal studies were conducted under the approval of the Institutional Animal Care and Use Committees of Genentech Lab Animal Research and were performed in an Association for the Assessment and Accreditation of Laboratory Animal Care (AAALAC)-accredited facility.

Note that full information on the approval of the study protocol must also be provided in the manuscript.

Clinical data

Policy information about clinical studies

All manuscripts should comply with the ICMJE guidelines for publication of clinical research and a completed CONSORT checklist must be included with all submissions.

Clinical trial registration	*Provide the trial registration number from ClinicalTrials.gov or an equivalent agency.*
Study protocol	*Note where the full trial protocol can be accessed OR if not available, explain why.*
Data collection	*Describe the settings and locales of data collection, noting the time periods of recruitment and data collection.*
Outcomes	*Describe how you pre-defined primary and secondary outcome measures and how you assessed these measures.*

Plants

Seed stocks	*Report on the source of all seed stocks or other plant material used. If applicable, state the seed stock centre and catalogue number. If plant specimens were collected from the field, describe the collection location, date and sampling procedures.*
Novel plant genotypes	*Describe the methods by which all novel plant genotypes were produced. This includes those generated by transgenic approaches, gene editing, chemical/radiation-based mutagenesis and hybridization. For transgenic lines, describe the transformation method, the number of independent lines analyzed and the generation upon which experiments were performed. For gene-edited lines, describe the editor used, the endogenous sequence targeted for editing, the targeting guide RNA sequence (if applicable) and how the editor was applied.*
Authentication	*Describe any authentication procedures for each seed stock used or novel genotype generated. Describe any experiments used to assess the effect of a mutation and, where applicable, how potential secondary effects (e.g. second site T-DNA insertions, mosiacism, off-target gene editing) were examined.*

Flow Cytometry

Plots

Confirm that:

☒ The axis labels state the marker and fluorochrome used (e.g. CD4-FITC).

☒ The axis scales are clearly visible. Include numbers along axes only for bottom left plot of group (a 'group' is an analysis of identical markers).

☒ All plots are contour plots with outliers or pseudocolor plots.

☒ A numerical value for number of cells or percentage (with statistics) is provided.

Methodology

Sample preparation	For pharmacodynamic analyses by FACS, mice were euthanized at day 7 after initial treatment. Tumors were dissociated into single cell suspensions by using gentleMACSTM dissociator (Miltenyi Biotec) and enzymatically digested in a buffer containing collagenase D (2 mg/mL) and DNAse (40 U/mL, Roche). Single cell suspensions of draining lymph nodes were obtained by mechanical dissociation through 40 µm cell strainers and performing red blood cell lysis as needed. Blood was obtained by terminal cardiac puncture and collected in lavender Microtainer Blood Collection Tubes (BD Biosciences, 365974) and subjected to red blood cell lysis. For detection of intracellular or nuclear staining by FACS, the FoxP3 nuclear staining buffer set (Invitrogen) was performed using recommended manufacturer's instructions. For intracellular cytokine detection, cells were stimulated for 4 hours with Cell Stimulation Cocktail (Invitrogen, 00-4870-93) at 37℃. For obtaining cells for single cell analysis, tumors and dLNs were processed into single cell suspensions as described elsewhere, and subjected to first tetramer staining, then surface markers and CITE-seq antibodies together. Processing of blood samples at day 0 before any treatment or at day 7 were first stained with hashed-tagged antibodies, then stained with surface markers.
Instrument	Cells were purified by fluorescence-activated cell sorting (FACS) on a Becton Dickinson FACSAria Fusion cell sorter equipped with four lasers (405 nm, 488 nm, 561 nm and 638nm). A 70-µm nozzle running at 70 psi and 90 kHz was used as the setup for each sort session. For flow analysis, All samples were acquired on LSR-Fortessa, BD Symphony Instruments (BD

	Biosciences) or Cytek Aurora.
Software	FACSDiva (V8.0.1), Flowjo (V10.8.1), SpectroFlo (V3.0.3)
Cell population abundance	Sorted cell purities were more than 95%.
Gating strategy	Examples of gating boundaries are provided as supplementary information. Boundaries were set against control samples (i.e. isotype or FMO samples) or based on density distribution.

☒ Tick this box to confirm that a figure exemplifying the gating strategy is provided in the Supplementary Information.